INVESTIGATION OF THE ELECTROCHEMICAL PROPERTIES OF HYDROXYAPATITE IMMOBILIZATION MATERIAL FOR POTENTIAL CYTOSENSOR FABRICATION

BY

ADUSEI DENNIS

(10472471)

A THESIS SUBMITTED TO THE SCHOOL OF GRADUATE STUDIES, UNIVERSITY OF GHANA, LEGON, IN PARTIAL FULFILMENT OF THE REQUIREMENT FOR THE AWARD OF DEGREE OF MASTER OF PHILOSOPHY (MPhil) IN BIOMEDICAL ENGINEERING

DEPARTMENT OF BIOMEDICAL ENGINEERING

COLLEGE OF BASIC AND APPLIED SCIENCES

UNIVERSITY OF GHANA

OCTOBER 2020

DECLARATION

I, ADUSEI DENNIS, do hereby declare that I have duly cited references used in this work, the entire work presented in this thesis, titled "INVESTIGATION OF THE ELECTROCHEMICAL PROPERTIES OF HYDROXYAPATITE IMMOBILIZATION MATERIAL FOR POTENTIAL CYTOSENSOR FABRICATION" was exclusively done by me and that, this thesis has never been presented either in part or in whole for any degree in this University or elsewhere.

..... 11-08-22

ADUSEI DENNIS (STUDENT) — DATE

..... 11/08/22

BERNARD OWUSU ASIMENG (PhD) (SUPERVISOR) — DATE

..... 12/08/2022

PROF ELVIS KWASON TIBURU (CO-SUPERVISOR) — DATE

ABSTRACT

Biomedical diagnostics is moving towards an effective and rapid diagnosis of which biosensor fabrication is the paradigm shift. Despite the successes obtained using sensing platforms, detachment of biorecognition elements from the transducing surface remains a hurdle to overcome. Good attachment of biorecognition elements to the transducing surface determines the sensitivity and specificity of the biosensor. In the area of cancer biosensing, gold, graphene, chitosan, and conducting polymers are among the few materials that have been exploited for effective immobilization, but they faced detachment problems. To curb these detachment problems, blends of cancer immobilizing materials and other molecules have been proposed but fabrication methods make the immobilizing material expensive. Thus, this thesis aimed at investigating the use of cost-effective hydroxyapatite (HAp) material synthesized from *Achatina achatina* snail shells (SHAp) for the direct immobilization of cells. SHAp was mixed with 3,4-ethylene dioxythiophene: poly 4-styrene sulfonate (PEDOT: PSS), a conductive polymer to increase the electrochemical responses of the SHAp forming a SHAp/PEDOT: PSS blend. The SHAp/PEDOT: PSS blend was used to modify a screen-printed electrode (SPCE) by a dropped coating approach after which cell-lines including pheochromocytoma (PC-12), human embryonic and kidney cells (HEK-293T) immobilized on the modified SPCE. Red blood cells (RBC) were used as a control. Cyclic voltammetry (CV) and electrochemical impedance spectroscopy (EIS) measurements were performed to record the cell proliferation signals. The CV results showed low peak currents for cell-lines (50 µA for HEK-293T and 120 µA for PC-12) and high peak current for the control RBC (230 µA). The EIS showed impedance values of 0.70 and 0.62 mΩ for HEK-293T and PC-12, respectively, and 0.52

mΩ for RBC. The findings demonstrate that SHAp is able to differentiate the proliferation signals of cells through potentiometric and impedimetric measurements. The unique current difference among these cells could be used as potential markers for the rapid detection of cancer cells at a low cost in future studies.

DEDICATION

In Love and Appreciation, this thesis is dedicated to OPANIN ABRAHAM KWAKU ADUSEI for your spiritual and financial support towards the execution of this work. Also, to my late Dad Mr Adusei Amponsem, Mr David Adu-Poku, the entire Adusei family and Mr Kweku Frimpong for your encouragement through words and kind.

ACKNOWLEDGEMENT

I am forever grateful to God Almighty for the wisdom, strength and protection throughout my academic journey in this institution. I extend my sincerest appreciation to my boss Dr. Francis Krampa for his benevolence, guidance and insightful comments that has transformed me this far. I take this opportunity to thank Prof Duodo Arhin for his willingness to allow me assess to his Raman spectroscopy whenever needed. Special thanks to my supervisors and all the lecturers in the Department of Biomedical Engineering, University of Ghana for their constructive criticisms during my thesis presentations. I am also grateful to the entire Protein synthesis lab at the West African Center for Cell Biology of Infectious Pathogens (WACCBIP), University of Ghana for the love shown me throughout my stay there. I am thankful to Miss Claudia Anyigba for her benevolence and unrelenting support during my cell culture procedures.

TABLE OF CONTENTS

LIST OF FIGURES

LIST OF ABBREVIATIONS

HAp – Hydroxyapatite

CHAp – Commercially acquired hydroxyapatite

SHAp – Hydroxyapatite prepared from snail shells

PEDOT: PSS – Poly(3,4-ethylenedioxythiophene):poly(4-styrenesulfonate)

SPCE – Screen printed carbon electrode

FTIR – Fourier transform infrared spectroscopy

EIS – Electrochemical impedance spectroscopy

CV – Cyclic voltammetry

R_{CT} – Charge transfer resistance

R_e – Electrolyte resistance

CPE – Constant phase element

I_{pa} – Anodic peak current

I_{pc} – Cathodic peak current

WE – Working electrode

CE – Counter electrode

RE – Reference electrode

W – Warburg impedance

POCT – Point of care testing

CT scan – Compuetrized tomography scan

MRI – Mangntic resonance imaging

ELISA – Enzyme linked immunosorbent assay

PCR – Polymerase chain reaction

PC 12 – Pheochromocytoma 12

HEK 293T – Human embryonic kidney transfection 293 cells

RBC – Red blood cells

CHAPTER ONE

INTRODUCTION

1.1 Background

A clinical cancer diagnosis is moving towards the development of analytical techniques that are very sensitive and specific in the rapid detection of biomarkers to provide point-of-care (POC) testing. Biosensors are recently being explored in the field of cancer as a rapid diagnostic tool with very high sensitivity and specificity. Biosensors have a low manufacturing cost, are portable, easy to use and, possess a low response time as compared to conventional techniques (Jayanthi, Das, & Saxena, 2017).

A biosensor consists of three main components: a recognition element (biocomponent or bioreceptor), a signal transducer, and a signal processor that relays and displays the results in an electrical or digital form. The recognition element determines the selectivity of the biosensor by recognizing the bioreceptor to produce a physiochemical signal, whereas the transducer determines the sensitivity of the biosensor by converting the biological response generated by the interaction of biorecognition molecules (cells, antigens, enzymes, antibodies, DNA/RNA) with the analyte into a measurable electrical signal (Tothill, 2009). Biorecognition molecules are immobilized to serve as a bridge between the recognition element and the transducing surface. Some of the biorecognition molecules require immobilizing materials to help increase the electrochemical reactivity of transducers as they help the biorecognition molecules to attach well to the transducer surface for energy transfer (Naseri, Fotouhi, & Ehsani, 2018).

Cytosensors, a cell-based biosensor, can make use of electrochemical techniques in their detection routes. The electrochemical cell-based detection system promises to be very sensitive and exhaustive as it gives great details of functional information about the target analyte (Bahadır & Sezgintürk, 2016). Electrochemical biosensors are confronted with challenges such as detachment of immobilizing material and which affects the analytes to release the precise biological signal for sensing by the transducer and thus, narrowing the range of detection (Naseri, Fotouhi, & Ehsani, 2018). Biomaterials such as graphene, chitosan, collagen, conductive polymers, and other inorganic materials are utilized as immobilizing materials in cancer biosensing to curb the detachment problem, but the fabrication methods are laborious and expensive. Thus, this thesis aimed at investigating the use of cost-effective hydroxyapatite (HAp) material synthesized from *Achatina achatina* snail shells (SHAp) for the direct immobilization of cells for potential cancer-based cytosensors.

Hydroxyapatite [HAp: $Ca_{10}(PO4)_6(OH)_2$] is an inorganic material that is obtained naturally from shells, bones, teeth, corals, and other calcium apatite or calcium phosphate deposits. HAp can also be obtained from synthetic sources for commercial purposes. HAp is biocompatible and has a wide range of applications due to its structural and chemical properties. For biomedical purposes, it is used in drug delivery systems, bone tissue scaffolding, bone and teeth filling, and coating of implant devices. It has been also used for environmental remediation purposes (Asimeng, et al., 2018). Literature reports that HAp can inhibit cancer cell proliferation and induce apoptosis in several cancer cells including osteocytes, colon cells, breast cells, and liver cells without affecting normal cells (Asimeng, et al., 2018), (Uskoković & Uskoković, 2011).

The HAp was prepared from *Achatina achatina* snail shells and phosphate-containing solution (SHAp) and the material structure was characterized using X-ray diffraction, Fourier

transform infrared, and spectroscopy Raman spectroscopy. For diagnostic purposes, 3,4-ethylene dioxythiophene: poly 4-styrene sulfonate (PEDOT: PSS) a conductive polymer with good electrical conductivity is introduced to form a SHAp/PEDOT: PSS blend, to increase the electrochemical responses of the SHAp. The SHAp/PEDOT: PSS blend was coated (modified) on screen-printed carbon electrodes (SPCEs) and cells immobilized directly on the modified SPCEs. Electrochemical studies were performed on the cell-seeded electrodes using cyclic voltammetry and impedance spectroscopy.

1.2 Problem Statement

Conventional cancer detection depends on the use of magnetic resonance imaging (MRI), computerized tomography (CT) scan, ultrasound etc. The conventional methods are faced with slow detection time, which hinders proper diagnosis and management of cancer patients. Laboratory procedures such as enzyme-linked immunosorbent assay (ELISA) and polymerase chain reaction (PCR) were also eliminated for detection because of the laborious processes and high involves. The conventional procedures are laboratory-based and involve skilled personnel. Thus, the procedure cannot be adopted as a point-of-care (POC) test. However, electrochemical biosensors (ECBs) have been considered for POC testing but ECBs are faced with the high cost of producing cancer immobilization molecules for the biosensor's detection. Thus, this study focuses on the investigation of the electrochemical properties of local-sourced SHAp as a cost-effective material for cellular immobilizing material in cytosensors.

1.3 Hypothesis

It is expected that the snail shell hydroxyapatite (SHAp) will show good electrochemical properties as compared to commercial HAp (CHAp) because of the carbonate-rich source the snail shells provide. It is expected that the SHAp will be more reactive to the cells than CHAp. The good attachment between the immobilizing material and the cells on the electrode surface will generate the precise signal for sensing by the transducer.

1.4 Study Aim and Objectives

The project's aim is to investigate the use of HAp prepared from snail shells (SHAp) as an immobilizing material for the development of a cell-based electrochemical biosensor. The SHAp would be used to modify electrode surfaces with a commercially acquired HAp (CHAp) as its control. To achieve the aim of this project, the specific objectives are to:

1. Determine the structural and electrochemical properties of CHAp and SHAp before and after coating on the screen-printed electrodes (SPCEs) surface.
2. Evaluate CHAp and SHAp immobilizing properties after cellular seeding on modified SPCEs surfaces.

1.5 Significance of the study

This research project will solve the complexities in the detachment of the immobilization of biorecognition elements and promote sensing transducer sensitivity. In addition, it will serve as a cost-effective way of providing potential POC testing for cancer.

1.6 Thesis Report Organization

This thesis is organized into six chapters; chapter one gives a brief description of the background of the project, addressed the research problems and outlines the specific objectives. Chapter two presents the history of biosensor research, types of biosensors, and their immobilization requirements and further explains literature works reported in electrochemical biosensing and some fundamental definitions, the structure of HAp and its relation to cancer cells. Chapter three gives detailed procedures on the materials and methods used for the study. Results were then presented in chapter four and the results are further discussed in chapter five. Chapter six provides conclusions and recommendations of studies.

CHAPTER 2

LITERATURE REVIEW

2.1 Introduction

This chapter gives a descriptive review of the literature encompassing the essence of cancer research, the properties and usage of hydroxyapatite, and biosensor fabrication and its related topics regarding cancer cell detection.

2.2 Global burden of cancer

Cancer is a significant cause of death, a disease of onus worldwide. It affects several millions of people across the globe and eventually killing more than half of its patients. The incidence of cancer is quite intriguing as it's been ranked as the second most likely cause of death preceded by the cardiovascular disease worldwide. With significant breakthroughs in monitoring cardiovascular-related conditions, cancer is predicted to become the leading cause of death worldwide in the nearest possible time. (Parkin, Bray, Ferlay, & Pisani, 2005)

The International Agency for Research on Cancer (IARC) a highly skilled agency for cancer studies at the World Health Organization, is periodically conducting an analysis of cancer incidence and mortality across the globe, in its global cancer burden, Globocan reports. Data from Globocan 2002 showed that there were 10,862,496 new recorded cancer cases (not including superficial cancer), of which more than half of the patients died. 5,801,839 (53.4%) of these cases were from men, and 5,060,657 (46.6%) were from

women of varying ages. Of the total number of new cases recorded, Asia had 45% of these new cases, Europe 26%, North America 15%, Latin America 7%, and Africa with 6% representing the least number of new cancer cases. Lung cancer recorded the highest incidence number of (965,446 male and 386,875 female cases a year) worldwide. It was followed by colon cancer (550,513 males and 472,743 females) and stomach cancer (603,003 males and 330,290 females) worldwide. Breast cancer was the most common cancer site among females (1,152,161 new cases a year), and then cervix (493,100 cases a year), and colon (472,743 cases a year). Males recorded lung cancer (965,446 cases a year), prostate cancer (679,060 cases a year), and stomach cancer (603,003 cases a year) as the most predominant cancers, respectively. It was projected that there would be about a 20% increment in the incidence rate of cancer cases in the year 2010 in the Globocan reports. (Ma & Yu, 2006)

Data from IARC in its Globocan 2012 suggest an estimated number of about 14.1 million newly recorded cancer cases, of which 8.2 million deaths were recorded, representing about 58% mortality. Unsurprisingly, it was consistent with the prediction from the Globocan data report in 2002. Current data from Globocan in 2018 reported an estimated number of 18.1 million new cancer cases, of which 9.6 million resulted in deaths representing about 53% chances of mortality from cancer. It can hence be deduced that one out of two cancer patients die. Prostate cancer was reported as the most dominant cancer type among males; meanwhile, lung cancer remained the highest cause of death among cancer patients. Breast cancer consistently was the predominant type of cancer in females as it also recorded the highest cause of death among cancer patients (Ferlay, et al., 2019). The incidence of cancer worldwide is expected to rise exponentially. Globocan projections by the year 2030 predict

an increase to 26.4 million cancer cases with 17 million resultant deaths. (Are, et al., 2013) The rise in these numbers presupposes the importance of research into curbing this growing global menace.

2.3 Causes of cancer development

From the resolution concerning the myth of cancer development over the years, several factors have been linked to cancer's potential causes. Cancer is caused by biological or internal factors, environmental exposures, occupational risk hazards, lifestyle-related factors, and several viruses and other infectious pathogens.

Biological factors such as age, gender, inheritable genetic and epigenetic defects, and race have all been shown to have some underpinning relation with cancer causes. Cancer is becoming a disease of old age as incidence tends to increase with increasing age making less developed countries stand a potential risk for higher cancer incidence due to a higher rate of population aging (Are, et al., 2013). It has been estimated that before the age of 75 years, the average risk of 20% of the population would have acquired cancer, and 10% of this number would have lost their lives (Ferlay, et al., 2019). Cancer incidence also tends to be higher among males worldwide to the female population worldwide (Kim, Lim, & Moon, 2018). Males recorded a risk of 20% incidence and a 40% mortality rate as compared to females (Siegal, Miller, & Jemal, 2014).

Changes in individuals' genetic and epigenetic makeup can be attributable to the development and progression of cancer in humans (Sadikovic, Al-Romaih, Squire, &

Zielenska, 2008). These alterations may be due to gene expressions or other genetic mutations (Sadikovic, Al-Romaih, Squire, & Zielenska, 2008).

Environmental exposures such as ultraviolet radiation from sunlight have all be showed to be risk factors for developing cancer. Carcinogenic materials such as tobacco, carbon monoxide, asbestos, and other radioactive materials all increase cancer development risk. Occupational hazards have also been attributed to the development of cancer (Blackadar, 2016). In the nineteenth century, a study revealed osteosarcoma development in women working on the painting of watch dials with radium (Martland, 1931). This study further supports radiologists' skin cancer development due to X-ray machines emitting radiations (Porter & White, 1907). It has been recognized that personal lifestyle decisions also contribute to cancer development (Futreal, et al., 2004). Poor lifestyles concerning health matters, nutrition, physical activities, and the consumption of supplements for various reasons have had adverse effects in cancer development (Blackadar, 2016).

2.4 Methods for the detection of cancer

Extensive research is ongoing to fast-track advancement into early and rapid detection of cancer and effective treatment to increase survival chances (Torre, et al., 2015). Several procedures/methods are being employed to increase the chances of early detection. Mostly, detecting and recognizing the signs and symptoms that indicate cancer dramatically improves treatment chances (Lingen, Kalmar, Karrison, & Speight, 2008).

Symptoms such as detecting lumps, sores, and abnormal bleeding may be pointing to cancer and must be investigated swiftly (Schiffman, Fisher, & Gibbs, 2015).

Screening thus, testing healthy people to determine those with cancer but have not yet presented with symptoms is a very effective way of detecting the presence of several forms of cancer at an early stage. Some methods of screening/detection of cancer are using mammography screening and cytology screening as a method to detect breast and cervical cancer, respectively (Hoerger, et al., 2011).

There are several methods used in diagnosing cancer. The clinician may perform a physical examination where he/she feels areas of the body for lumps or examine for discoloration and enlargement, which may indicate cancer. Laboratory investigations such as urine and blood tests may also be done to look for the presence of abnormalities (tumor biomarkers) that may have been caused by cancer. Detection of cancerous cells from normal cells is based on the differentiation or classification of their intracellular and extracellular markers (Bajaj, et al., 2009). Again, imaging tests may be carried out to noninvasively view and examine the internal organs to look for signs of tumors. Examples of imaging modalities used are CT scans, MRI scans, PET scans, X-rays, ultrasounds, and many others. Also, samples of cells and/or tissues may be collected through a process called biopsy, which is then tested in the laboratory for cancer (Lingen, Kalmar, Karrison, & Speight, 2008).

Detection of cancer using the presence of tumor biomarkers in blood, urine, cerebrospinal fluids, and other bodily fluids is one of the standard methods that have been used for years now. Even though this method has been used for decades, its effectiveness is questionable, especially in identifying some common cancers. For example, Prostate-Specific Antigen (PSA), a biomarker used to ascertain the presence/onset of prostate cancer, has been found to produce cancer-like positive results in men who would never have developed prostate cancer, placing them at higher risk of morbidity as a result of the unnecessary prostate

cancer treatment. Antigens CA-15.3 and CA-27.29, which are routinely used to determine the recurrence of breast cancer, though more accurate than PSA, do not result in any substantial increase in chances of survival or quality of life (Molassiotis, Wilson, Brunton, & Chandler, 2010).

Radiology to screen for cancer has also been used for many years with high effectiveness and benefits in the early detection of breast cancer, colorectal cancer, and Lung cancer. However, even with its relatively high success rate, radiographic imaging still produces false positives leading to unnecessary and, most times, painful treatments.

Using the presence of Circulating Tumor DNA (ctDNA) to detect Circulating Tumor Cells (CTC) has become well known and attractive over the years due to the potential of using the test to screen for multiple types of cancer simultaneously, especially for those cancers that have no medium for early detection. A challenge with this method, however, is identifying the source of the positive test, i.e., which specific cancer is present (Molassiotis, Wilson, Brunton, & Chandler, 2010).

Biosensors are recently being explored in the resolution of the detection of cancerous cells due to its high sensitivity and specificity as compared with the other conventional methods (Jayanthi, Das, & Saxena, 2017).

2.5 Hydroxyapatite

Hydroxyapatite, an inorganic material, has been used as a biomaterial in several fields, from environmental purposes such as water treatment to the medical setting. Over the last two decades, the literature points to the vast usage of HAp for biomedical purposes. Due

to the resemblance of HAp to the calcium apatite component of bones, HAp has been utilized in bone scaffolds in tissue engineering as well as bone and teeth fillings. Drug delivery, cell targeting, bioactive coatings, and genetic related researches have all explored the prospects of HAp. For diagnostic purposes, HAp has been utilized in biosensor fabrications (Vakili, et al., 2020), label-free fluorescence, and imaging studies (Lin, 2015).

HAp has a molecular formula of [HAp: $Ca_{10}(PO4)_6(OH)_2$] with functional groups CO_3^{2-}, PO_4^{3-}, and OH^- (Asimeng, et al., 2018). It usually possesses a hexagonal crystal structure comprising an array of tetrahedral PO_4^{3-} bonded together by CO_3^{2-} interspersed within the structure. CO_3^{2-} is positioned along aligned columns and on its axes, with OH^- pointing adjacent to it (Ma & Liu, 2009), (Lin, 2015). It has a space group $P6_3/m$ with a, b, and c-axis where HAp unit cells are arranged along its c-axis, which is preferred for its orientational growth. HAp can also appear monoclinic with a $P2_1/b$ space group where OH^- groups are oriented, pointing in the same direction in a given column, unlike in its hexagonal form with OH^- pointing in opposite directions (Ma & Liu, 2009). The HAp in its hexagonal structure is mostly prepared through precipitation of supersaturated HAp solutions at 25–100^0 C. The monoclinic HAp is prepared by the heating of hexagonal HAp at 850^0 C in air and cooling at room temperature. The a and b axis planes of HAp possess a positive charge, hence tend to adsorb negatively charged molecules. In contrast, the c-axis plane carries a negative charge; therefore, adsorb positively charged molecules onto its planes. HAp molecules are ionically balanced with a net charge of zero but tend to shift in charge when placed in an ionically imbalanced environment.

HAp can undergo ion-substitution with trace elements such as Mg, Na, Zn, F, Cl, and carbonate on its crystal lattices during preparation (Gómez-Morales, Iafisco, Delgado-

López, Sarda, & Drouet, 2013), (Uskoković & Uskoković, 2011), (Lin, 2015). (Asimeng, et al., 2018) demonstrated the preparation of a unique type B and type AB HAp which had undergone carbonate and sodium substitutions through chemical precipitation. Varying the stirring time affected the crystallinity and concentration of trace elements on its surface, where it was applied in the removal of fluoride ions from water (Asimeng, et al., 2018). The temperature has an influence on the crystallinity of HAp particles. This was demonstrated by a work done by (Murugan & Ramakrishna, 2005), where the HAp crystal nature increased when heated at 900^0C.

The particle size, shape, crystal nature, structure, and chemical composition of HAp have an influence on its properties hence its application. Nanosized HAp particles have greater efficiency than its microscale structures in their sintering ability, bioactivity, resorbability, and higher mechanical property. HAp sizes and shapes as well as its porosity have an influence on the efficiency of drug loading and delivery, cell targeting and diagnosis, and gene transfection. Ion substitution changes the chemical composition of HAp, an essential role in increasing the biological responses of apatites, improving the solubility and degradation rate of HAp particles of which carbonate CO_3^{2-} has the most significant. Carbonate-ion substitution usually occurs by replacing OH^- or PO_4^{3-} ions on its tetrahedral sites with CO_3^{2-} ions to form A- or B-type carbonate apatites, respectively (Lin, 2015) (Asimeng, et al., 2020).

2.5.1 HAp and cells

Several studies have established the interactions between several functional groups of HAp and other bio elements such as hemoglobin, nuclear components, enzymes, antibodies, and several carboxylate groups (Zhao, Xu, Zhang, Zheng, & Zheng, 2010). HAp is known to

have an adhesive interaction with sialic acid, a carbohydrate molecule found on cell surfaces, of which cancer cells are included. The phenomenon for this interaction has not been exhaustively understood in literature (Barnard, et al., 2019) (Luukkonen, et al., 2019). (Asimeng, et al., 2019) Further elaborate the electrochemical effect of HAp on Hella cells in its study.

Sialic acid is a 9-carbon monosaccharide located on the terminal ends of glycan chains, glycoproteins, glycolipids, and glycopeptides. Sialic acid can be found on cell membranes' surface and in the cell's internal organ secretions evident in plasma concentrations (Barnard, et al., 2019). Expression of sialic acid is present on all cell types of vertebrates but limited to selected higher invertebrates modulating a series of normal and pathological conditions. It possesses a net negative charge with hydrophobic properties, aiding its activities differently in normal and pathologic processes, acting as binding sites for various toxins and pathogens. They influence hormonal functions and behavior, assisting in the catalytic cycles of enzymes, adhesion and interaction of cells, as well as molecular recognition and its transport mechanisms. Cells at different body sites exhibit differences in sialic acid content, with human brain cells containing the highest content (Mehdi, Singh, & Rizvi, 2012). Cellular senescence and changes in its carbohydrate structures has an effect on sialic acid expression. Sialic acid has been reported to increase in quantity and have an effect on the progression of tumor cancer cells into its metastatic stage due to its high expression in glycoproteins. It ensues a higher negative charge on the cancer cell surfaces resulting in the repulsion of cells leading to its leakage into blood or urine (Gong, et al., 2015).

2.5.2 Polarization and Depolarization in biological cells

There is substantial evidence of differences in the electrical behavior of cells imposed on their cell membranes. It has been reported from literature that, cells; normal or cancerous, have electrochemical properties which is due to the formation of an electrochemical gradient across their cell membranes. This can be attributed to the unequal number of charges of ions or electrons in their intracellular and extracellular environs. A normal cell undergoes polarization of ions (efflux of Na^+ and the influx of K^+ to the cytoplasm) and subsequently tries to obtain a resting potential by balancing its ion concentrations across their plasma membrane. Meanwhile, cancerous cells undergo an irreversible depolarization of ions (influx of more Na+ ions leading to the imposition of a negative charge onto the cytoplasm) across their plasma membranes. Polarization and depolarization of ions generate membrane potentials needed for cellular communications. The stimuli generated through depolarization are very strong and communicate faster, hence the rapid proliferation of cancerous cells (Lodish, et al., 2000), (Yang & Brackenbury, 2013).

2.6 Biosensors

Sensor development is very essential in the fabrication of analytical devices for the detection, analyses and monitoring of specific chemical determinants in substrates. These sensors contain an active sensing platform which can be classified as either chemical sensors or biosensors. Biosensors operate based on sensing platforms which can detect biochemical compounds such as proteins (antigens, antibodies, enzymes), cells, nucleic acids, tissues, and other metabolites from physiological and pathological reactions in the human body. Biosensors have also been applied in the food and drug industries for the

detection of harmful organisms and chemicals in water, air, food products, and drugs for environmental and health purposes. For the purposes of combatting crime and warfare, biosensors are used in the design and detection of biological and chemical weapons. (Bohunicky & Mousa, 2011). Generational developments and research in the biosensing industries is to improve the current state and function of biosensors.

2.6.1 Types of biosensors

Biosensors are made up of three intimately joined components in its fabrication; a biorecognition element fused with a transducer connected to a signal detector which relay and process the signals into a measurable form. Biosensors are mostly categorized into optical biosensors, piezoelectric biosensors, and electrochemical biosensors based on the type of transducing platform used. Several transducers or working electrodes (sensors) can be interfaced to a single biorecognition element to transform the biosignals into an electrical or digital form for quantification, display and analyses (Zhang, Guo, & Cui, 2009).

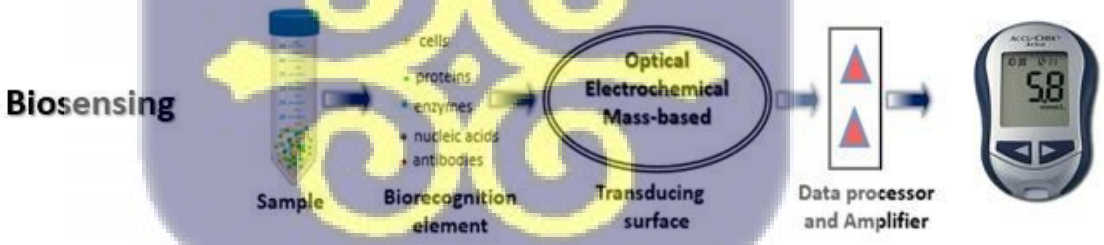

Figure 1 A schematic illustration of a biosensor

2.6.2 Optical biosensors

Optical biosensors utilize alterations in light radiations to measure changes in their specific wavelengths. Optical transducers make use of light absorption, luminescence, fluorescence, total internal reflection, colorimetric, interferometry or surface plasmon resonance (SPR) to identify biomolecules. It relies on changes in the wavelength in response to the detection of biomolecules and converts these signals into an electronic or digital form (Bohunicky & Mousa, 2011), (Jerónimo, Araújo, & Montenegro, 2007).

In these optical biosensors, optical fibers and waveguide devices are used to improve detection sensitivity by increasing the interaction between the guided light and the sensor surface. This type of biosensors has been exploited in areas of cancer research using antibody labeling detection methods as they are also capable of multiplex detection of targets. (Anderson, et al., 2017), (Fan, Lu, Wang, & Liang, 2008). Over the recent years, optical biosensors have been improved and used for several research such as the application of SPR biosensors in the detection of cancer biomarkers. Nanotechnology applications in conjunction with surface chemistry analysis were applied in lung cancer detection where dendrimer molecules were used in the SPR biosensor (Altintas & Tothill, 2013) (Altintas, Uludag, Gurbuz, & Tothill, 2012). Surface-enhanced Raman Scattering method is another example of optical biosensing which is being investigated to having a superior advantage over the fluorescent based procedures for nucleic acid biomarkers in cells for the purposes of cancer detection (Nolan, et al., 2012), (Ouyang, Hu, Zhu, Cheng, & Irudayaraj, 2017). (Yildiz, Alagappan, & Liedberg, 2013) Demonstrated the use of optical biosensors as a point-of-care testing tool for cancer related complications. It employs the use of the naked eye for cancer detection using a luminescent reporter for a paper based optical biosensor.

2.6.3 Mass-based biosensors

Biosensors containing mass-based transducers include piezoelectric and acoustic wave biosensors. Piezoelectric biosensors operate by generating frequencies due to changes in the mass of crystals when a potential is applied across. Signals generated are then converted into readable formats. This class of biosensors has widely been explored in the field of cancer detection (Bohunicky & Mousa, 2011). Piezoelectric technology was utilized by in conjunction with PCR amplification technology for the detection of the p53 gene; a very crucial gene in cancer proliferation. Alpha-feto-protein (AFP) another molecular biomarker for cancer was also detected by using nano-sized particles of hydroxyapatite and gold nanoparticles (Jayanthi, Das, & Saxena, 2017), (Ding, Li, Wang, & Chen, 2016). Quartz crystals are the most commonly used crystal type due to its superior chemical, mechanical and electrical properties. For analytical purposes, it has been used in the detection of viruses, cells, antibodies, and other disease biomarkers (Altintas & Tothill, 2013).

2.6.4 Electrochemical biosensors

Electrochemical biosensors are a category of biosensors which are relatively very cheap, easy to handle and operate, as well as portable compared to its competitors. This makes it the choice of biosensor commonly used in the medical setting for diagnostic purposes. Transducers in electrochemical biosensors have been fabricated into semiconductors and screen-printed electrode platforms for rapid diagnostics. Electrochemical amperometry biosensors operate on the principle of measuring the current generated when a potential or voltage is applied across electrodes in a chemical reaction. These reactions are mostly redox in nature due to the transfer of electrons between electrolytes and electrodes in a

system producing electrical current. Amperometric transducers have proven futile in genetic sequencing to determine gene mutations in association to cancer, hence relevant in its detection. It has been applied in the production of noninvasive wrist glucometers. This biosensor picks glucose signals from the skin surface and converts it into an electrical signal to be read digitally in real time (Bohunicky & Mousa, 2011), (Wang & Kawde, 2001), (Koschwanez & Reichert, 2007). Potentiometric biosensors are another class of electrochemical biosensors which operates using an ion selective electrode to detect biorecognition elements by converting their presence or level into electrical signals to be measured. An example is the light-addressable potentiometric sensor (LAPS) linked with a phage recognition element for breast cancer detection (Bohunicky & Mousa, 2011).

Impedimetric biosensor is another group of biosensors of great interest due to its emerging great impact in the field of rapid and effective diagnosis. It makes use of the resistance and capacitance encountered when an alternating current is applied across a transducing surface during biological reactions for its detection. These reactions involve the flow of electrons which face resistance from both internally controlled and external sources. This gives us the opportunity of detecting these biorecognition molecules without necessarily the use of labels such as enzymes. Impedimetric biosensors have been explored substantially in the field of immunosensors and aptasensors. HER-3, a human epidermal growth receptor that can be associated with breast cancer and its treatment, was first quantified by (Canbaz & Sezgintürk, 2014) using anti-HER-3 as the target. They applied a single impedance technique, using gold nanoparticles immobilized on a gold electrode to form the immunosensing transducing platform. Regan et al. 2014 worked on electrochemical aptamer-based biosensors (genosensors) for impedimetric nucleic acid detection. This

genosensor proved to be inexpensive but very sensitive and requires fewer procedures, unlike the conventional PCR methods available (Bahadır & Sezgintürk, 2016).

2.6.4.1 Cytosensors

Cytosensors, a cell-based biosensor, can make use of electrochemical impedance techniques in detection systems using various cell classifications. This detection system promises to be very sensitive and exhaustive as it gives great details of functional information about the target analyte. This can be greatly referenced to the structural configuration and constituents of the cell membrane of most cells; prokaryotic and eukaryotic cells structure. These cells are electrically active, variably in nature for their survival (Bahadır & Sezgintürk, 2016), (Asimeng, et al., 2019). Qualitative and quantitative detection and monitoring of bacteria cells using a cell-based biosensor has been established by (Qi, Wan, & Zhang, 2013) as well as the use of impedimetric techniques to successfully study the bio-behavior of cancer cells in respect to detection approaches been investigated (Liu, et al., 2009).

2.7 Immobilization techniques in biosensor fabrication

The successful transfer of biorecognition molecules or analytes understudy onto the transducing surface known as immobilization is a very critical step in the provision of a good biosensor. This step determines the accuracy, longevity, cost, and the response time of the biosensor as a rapid diagnostic test tool. Immobilization predicts the successful onset or completion of a chemical reaction needed on a transducing surface to yield the expected results such as, color, pH, temperature, and current. A good immobilization assures the embedment of biorecognotion molecules, preventing them from leaching out on the

transducing surface. This phenomenon helps prevent the obtainment of false negative results. It also helps in widening of the detection range limit of the biosensor due to good signal generation from the biorecognition element. The efficient transfer of electrons on an electrochemical transducing platform would only be possible when there is good communication between the electrode and the biorecognition element aided by the immobilizing material and technique used.

Adsorption, entrapment, covalent bonding, and cross-linking techniques are few of the famous immobilization techniques in biosensor fabrication. Adsorption and entrapment are generally considered as physical methods whereas covalent boding and cross-linking are regarded chemical means of immobilization (Jianrong, Yuqing, Nongyue, Xiaohua, & Sijiao, 2004), (Putzbach & Ronkainen, 2013).

2.7.1 Adsorption

Adsorption is the attachment of biorecognition elements onto its transducing surface physically through forces such as hydrophobic, electrostatic interactions, and Vander Waals bonding. Despite the successes of this technique as easy and fast, it is faced with challenges such as unsuitable transducing surface and biorecognition element orientation difficulties as well as reaction conditions which affects its existence. This technique even though mostly results in weak bond formation, it is the relatively used method in enzymatic biosensor fabrications.

2.7.2 Entrapment

Entrapment technique of immobilization refers to the localization of biorecognition elements into a polymer matrix or gel onto a transducing surface for its identification. This

technique, despite mostly used in cell immobilization, is mostly applied in enzyme immobilization for its retainment. Few challenges confronting this technique is the inactivation of some enzymes and its limitations in diffusion. This challenge could be resolved by modifying the matrix being used.

2.7.3 Covalent bonding

Covalent bonding technique of immobilization is one of the frequently used methods. It involves the interaction between functional groups of the biorecognition elements and that of the immobilizing materials bound to the transducing surface. Enzymatic biosensors have showed much success in the application of this technique. Functional groups usually explored in this methodology are carboxyl groups, amino groups, hydrophobic as well as the phenol groups.

2.7.4 Cross-linking

Cross-linking technique of immobilization involves the joining of large or whole molecules of biorecognition elements to form a larger molecule of a complex 3-dimensional structure. This process is mostly done by the formation of covalent bonds between the biorecognition elements through the use of bi- or multifunctional chemical reagents. This technique professes a stronger stability to the resultant biorecognition element (Jianrong, Yuqing, Nongyue, Xiaohua, & Sijiao, 2004), (Putzbach & Ronkainen, 2013).

2.7.5 HAp as an immobilizing material

(Vakili, et al., 2020) Successfully used HAp nanoparticles as an immobilizing material in an immuno electrochemical biosensor for the targeting and detection of ssDNA BK polyomavirus. This was due to the biocompatibility of HAp as well as its potential in

keeping biorecognition elements in their bioactive states, an important attribute of an immobilizing material. Moreover, HAps crystalline structure allows it to be redox active in nature and assist in the flow of electrons across its surface (Vakili, et al., 2020) (Asimeng, et al., 2019) (Zhao, Xu, Zhang, Zheng, & Zheng, 2010). HAp in its architectural forms; rods, tubes, and wires have been studied to have excellent properties when used as immobilizing agents for biosensors due to their crystalline states and their bigger surface area for adsorption of biomarkers (Farzin, Shamsipur, Samandari, & Sheibani, 2018). (Bharath, et al., 2015) explored the use of 1D HAp in enzymatic electrochemical biosensors for the successful detection of glucose. A lot of materials including several carbon nanomaterials, metals and its oxide derivatives have all been investigated as immobilizing materials (Farzin, Shamsipur, Samandari, & Sheibani, 2018).

The introduction of conductive polymers into electrochemical biosensor fabrication has become successful for diagnostic purposes. Conductive polymers are environmentally friendly, relatively less expensive, biocompatible and of high electrical conductivity especially when doped. An example is poly(3,4-ethylenedioxythiophene) (PEDOT) doped with poly(4-styrenesulfonate) (PSS), forming a PEDOT: PSS compound with a good electrical conductivity and portraying excellent mechanical properties and stability. PEDOT: PSS has been applied in several biosensor fabrications (Krampa, Aniweh, Awandare, & Kanyong, 2017), (Sheng, Xu, Xu, Wang, & Luo, 2015). Nanocomposites are usually formed from the addition of various conductive polymers with biomaterials to increase the electrochemical properties of the biomaterials. Often conductive polymers are used in conjunction with some biomaterials to form nanocomposites with the intent of complimenting the biomaterials as good immobilizing material, such as lowering the

processing temperature of the resultant nanocomposite (Putzbach & Ronkainen, 2013) (Zhang, Guo, & Cui, 2009). From literature it is indicative that HAp has been used alone in some biosensor research (Zhang, Chen, Xie, & Liu, 2009), but it's mostly used in a nanocomposite form or conjunction with metallic components such as copper, lead, calcium, cadmium, and zinc to increase its adhesive properties as well as increase its surface energy and surface area for ion transfer for electrochemical purposes (Zhang, Guo, & Cui, 2009).

2.8 Electrochemical evaluation techniques

Electrochemical biosensors basically operate on the principle of electrochemistry where electron transfer mechanisms are studied for the detection of target biomarkers or products. It probes reactions involving the transfer of electrons, thus their redox reactivities; oxidation and reaction. The electron exchange takes place in a cell, which consists of an external power source such as a galvanostat or a potentiostat, an electrode which is an electrically conductive material; glassy carbon, gold, silver, mercury, platinum, and an electrolyte to serve as a bridge. A voltage serving as a driving force is applied across an electrode which excites electrons in the electrode. Electrons of higher energy levels exit the electrode and interact with electrons in the electrolyte creating an energy difference. The flow of the electrons generates current proportional to the concentration of redox reactive analytes present. Below are some electrochemical techniques for analyzing the dynamics of redox reactions taking place in an electrochemical biosensor.

2.8.1 Cyclic voltammetry

Cyclic voltammetry is very essential in the fabrication of biosensors. It allows us to analyze the redox behavior; oxidation and reduction as well as showing whether a biomaterial goes through a reversible or irreversible redox reaction. A cycling potential is applied across an electrode to produce a resultant current which is reflective of the redox state of the biomaterial used. The conductivity of biomaterials is accessed using their peak currents extracted from their cyclic loop.

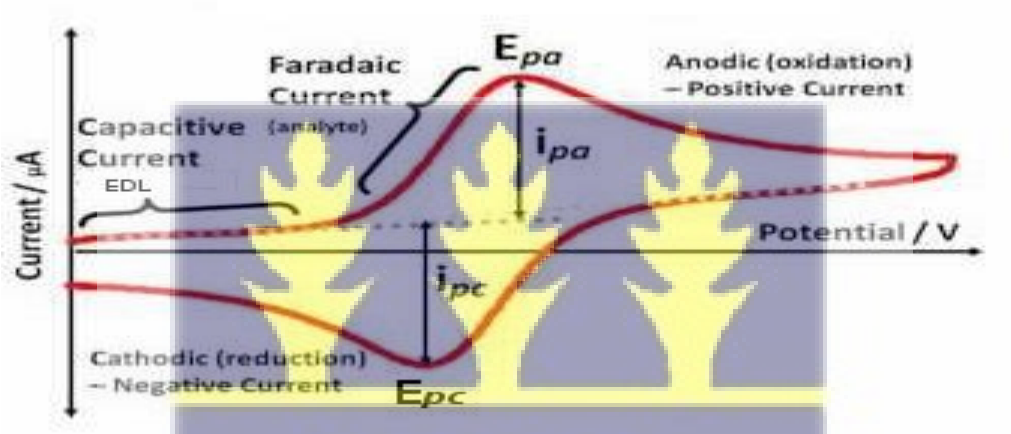

Figure 2 Cyclic voltammogram of a reversible redox reaction

(Skoog, Holler, & Crouch, 2017).

Following the Nernst equation, an equilibrium in the redox reaction activities can be explained. It helps to determine the changes in concentration of the species or potential across the electrode. $E = E^0 + \frac{RT}{nF} \ln \frac{(0x)}{(Red)} = E^0 + 2.302\theta \frac{RT}{nF} \log_{10} \frac{(OX)}{(Red)}$

E is the electrochemical cell potential

E^0 is the species standard potential

R is the Universal gas constant

T is the temperature

F is the Faradays constant

n is the number of electrons

2.8.2 Electrochemical impedance spectroscopy

Electrochemical impedance spectroscopy (EIS) is a sensitive technique in biosensor fabrication especially for label free and non-enzymatic detections. It's used in electrochemical research involving the study of electron transfer resistance occurring on the superficial and bulk solution of systems. It is relevant in surface characterization of transducing surfaces after modification with immobilizing materials and biorecognition elements particularly those with binding effects. It is not only used for analysis but also for analytical diagnostic purposes.

A cycling sinusoidal potential is applied across an electrode at varying frequencies to study the impedance to the resultant alternating current response. The impedance is represented as a function of voltage-time to current-time.

$$z = \frac{v_{(t)}}{I(t)} = \frac{v_o \sin(2\pi ft)}{I_0 \sin(2\Pi ft+\phi)}$$

V_o and I_o termed as its maximum voltage and current, frequency(f), time(t), and its phase shifts as (ϕ). The data can be represented on a Bodes plot or a Nyquist plot.

An electrical equivalent circuit (Randles) is generated in addition to the plot when the electrolyte gets contact with the electrode surface. The circuit with the spectrum gives an

experimental data to aid understand the impedance generated across the system. Parameters included in the circuit are an electrolyte resistance (R_e), charge transfer resistance (R_{CT}), the Warburg impedance (W), and the constant phase elements (CPE). R_e is referred to the resistance faced by the electron flow from the electrolyte whilst the R_{CT} is the resistance towards electron flow from the whole redox system and the electrode at the interface. Warburg impedance (W) is based on the diffusion of ions from the electrolyte to the electrode, which occurs at low frequencies. It is usually presented as a straight line inclined at an angle of 45^0 (Lisdat & Schäfer, 2008), (Dorledo de Faria, Iden, Heneine, Matencio, & Messaddeq, 2019).

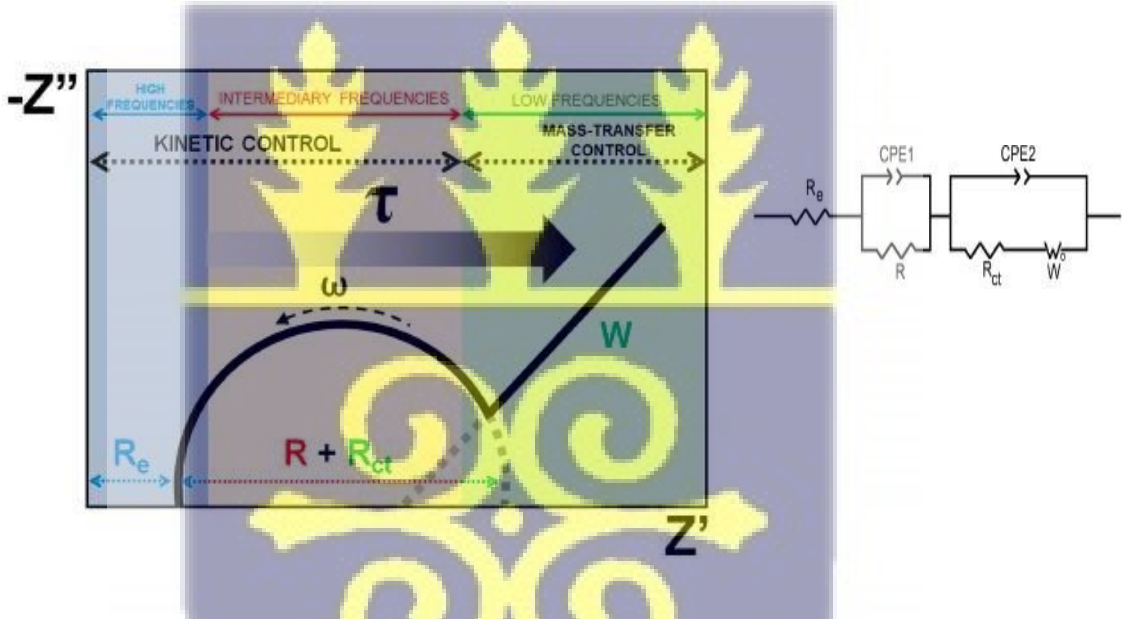

Figure 3 A Nyquist plot of an electrochemical cell with an equivalent Randles circuit.

(Dorledo de Faria, Iden, Heneine, Matencio, & Messaddeq, 2019)

2.9 Structural characterization techniques

The surface morphology and topography have been investigated in material sample analysis using several analytical modalities. It probes the particle size and geometry to

provide a definite information on the properties of the material. Other techniques have dominantly been applied in determining particle size or volume distribution, surface area and pore sizes which gives data on particles and reaction products formed. Instrumentations such as electron microscopy, optical microscopy, atomic force microscopy, X-ray diffraction, X-ray photoelectron spectroscopy, Fourier transform infrared, Raman spectroscopy are all used in structural characterization analysis (Upadhyay & Kumaraswamidhas, 2018).

2.9.1 Raman spectroscopy

This is spectroscopic technique applied to identify particles using their vibrational, rotational, and other low frequency states to detect their peculiar functional group fingerprints. This technique was named after C.V. Raman after he had discovered it in 1928. Modern Raman spectrometers have improved significantly with the use of a laser as source of excitation radiation. Here to, photographic plates and mercury lamps were used as sources of excitation radiation until the evolvement of a laser. This milestone has increased the performance of this spectroscopy by lowering capturing time due to stronger radiation source, increasing detection sensitivity resulting in a strong Raman scattering of molecules (Long, 2002).

Raman spectroscopy operates on the principle of utilizing the inelastic technique of incident radiation. A monochromatic light energy is incident on a sample where it interacts with its molecules, resulting in absorption, reflection or scattering of radiations. Raman spectrum consists of the scattered light with frequencies unequal to the incident radiation known as the Raman scattering which makes up the minority but of major importance to this technique. Majority of the scattered radiation had an equal frequency with the incident

radiation as is termed as the Rayleigh scattering. Frequencies are represented as stokes and anti-stokes when the frequencies of the scattered radiation are higher or lower than the frequencies of the incident radiation, respectively. The spectrum is measured using the laser line as a reference. Subsequently, the sample peaks are measured as a shift from the reference laser line. These peak positions are determined by the vibrational energies associated with the bonds or functional groups in the molecules of the sample constituents. The characteristic bands in the Raman spectrum are those that are due to highly polarizable bonds (Bumbrah & Sharma, 2016).

Raman shifts are usually presented as wavenumbers (cm^{-1}). Its formula is presented below;

$$D = \left(\frac{1}{a} - \frac{1}{b}\right) \times \left(\frac{10^7 nn}{cm}\right)$$

Where D is Raman shift (cm^{-1}), a is excitation wavelength (nm) and b is Raman spectrum wavelength (nm).

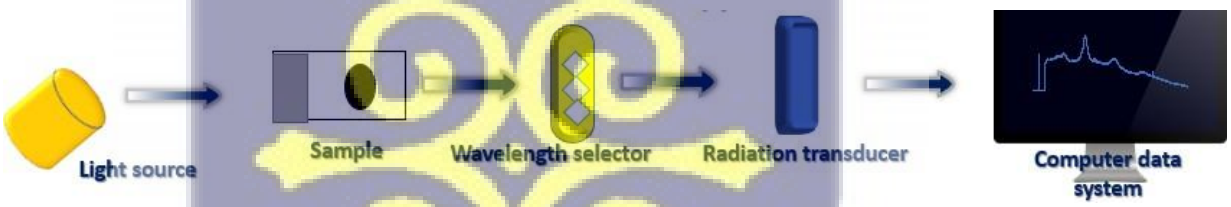

Figure 4 A diagrammatic illustration of the Raman spectroscopy technique

2.9.2 Fourier transform infrared (FTIR) spectroscopy

This is a spectroscopic technique for the quantitative detection and analysis of functional groups or chemical bonds between atoms of materials by measuring their vibrational frequencies. This technique has reportedly been used over seven decades as it has become common due to its less costive usage. FTIR also is a nondestructive technique which

utilizes infrared radiation just like Raman spectroscopy. Information retrieved in this technique is due to the interfacial vibrational dipole interaction of atoms since the incident light beam interacts superficially with the sample. Chemical bonds between atoms of molecules respond differently to infrared radiation. There is no infrared signal observation between carbon-sulphur bonds, unlike silicon-oxygen bonds which produces substantial signals even at sub monolayer levels of samples (Cox, 1992).

A sample is exposed to infrared radiation (incident) where the sample either reflects, transmits or absorbs some radiation. The wavelength frequencies of the incident infrared radiations which was reflected, transmitted and absorb by the sample is measured by the change in intensity of the resultant radiation in respect to wavelength. These changes in wavelength frequencies reflect the excitation of vibrations in dipole moments in chemical bonds which are specific to functional groups (Cox, 1992). The reflectance, transmission and absorbance are deduced respectfully using the following equations;

$$R_w = \left(\frac{R_T}{R_0}\right)_\omega \qquad (1)$$

R_0 is the intensity of the incident radiation R_T is the intensity of reflected radiation

R_w is the reflectance of samples at frequency w

$$T_w = \left(\frac{I_T}{I_0}\right)_\omega \qquad (2)$$

I_0 is the intensity of the incident radiation I_T is the intensity of transmitted radiation

T_w is the transmittance of samples at frequency w

Using the Beer-Lamberts law, absorbance can be related to the transmittance of radiation by;

$A_W = 2 - \log T_W$ (3)

A_W is the absorbance of samples at frequency w (Cox, 1992).

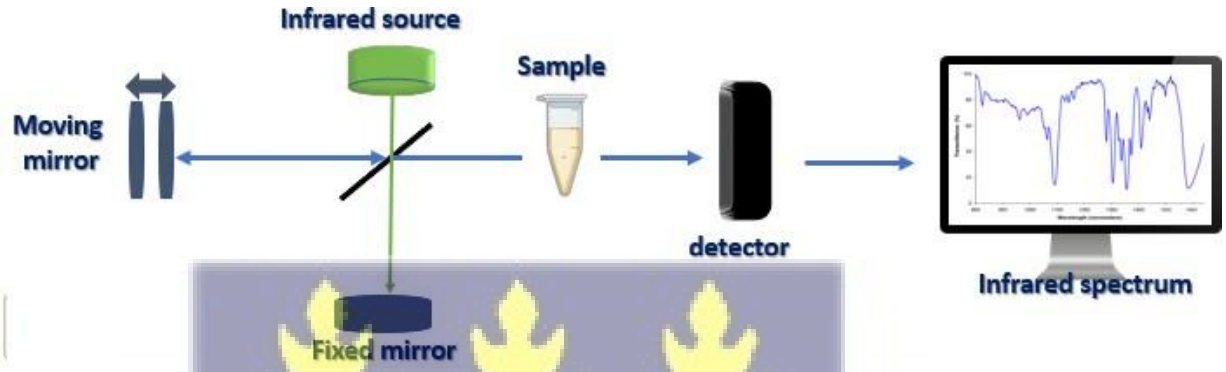

Figure 5 A diagrammatic illustration of the FTIR technique.

CHAPTER THREE

MATERIALS AND METHODS

3.1 Introduction

This chapter provides detailed information on the materials used in the project, the equipment utilized, sample preparation procedures, and the analytical techniques used.

3.2 Materials

Snail shell hydroxyapatite (SHAp) was obtained using Asimeng et al procedure (Asimeng, et al., 2019) at a calcination temperature of 850°C. The commercial HAp (CHAp), phosphate-buffered saline (PBS, pH~7.4), and Milli-Q high-grade ddH_2O were purchased from Sigma-Aldrich (St. Louis, USA). A redox probe (potassium hexacyanoferrate ferrocyanide (III)) was purchased from Sigma-Aldrich (St. Louis, China). A conductive polymer (PEDOT- PSS: (3,4-ethylene dioxythiophene)-poly(4-styrene sulfonate)) was obtained from Sigma-Aldrich (St. Louis, Belgium).

3.3 Methods

3.3.1 Synthesis of HAp

The *Achatina achatina* snail shells were cleaned adequately under running tap water to remove all impurities, after which it was dried for 6 hours under sunlight. The clean dried shells were grounded into powder and the powder calcined at 650, 750, and 850°C to eliminate any organic components in the shell powder and to transform the powder

structure to calcite. A volume of 0.3 M solution of diammonium hydrogen phosphate (DHP) was added in a dropwise manner to a molar volume of 0.5 M calcite and stirred for 1 h at 40°C using a magnetic stirrer. The solution's precipitate was filtered and dried at 100°C in an oven for 2 h to obtain HAp powders (Asimeng, et al., 2019). The synthesis route is illustrated in Figure 6.

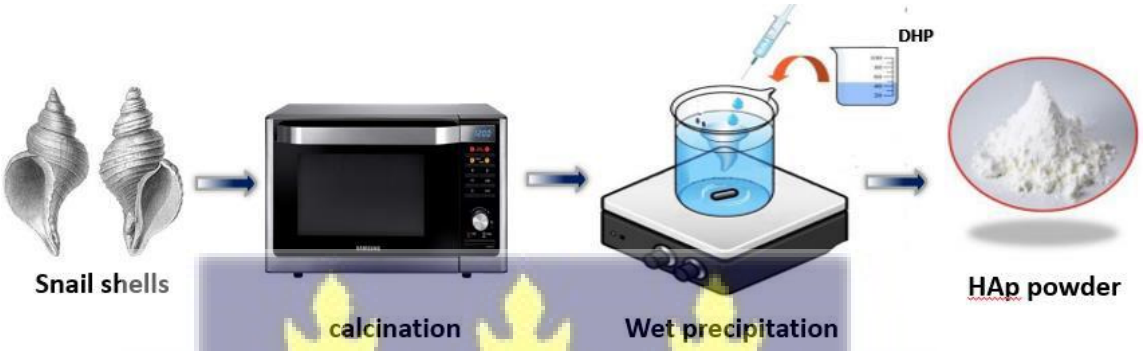

Figure 6 A schematic illustration of the preparation of SHAp. Snails' shells are grounded into powder, and the powder is heated in an oven to convert to calcite. The calcite powder is then mixed with DHP and stirred to produce SHAp powder.

3.3.2 CHAp and SHAp characterizations

The phase compositions of the commercial hydroxyapatite (CHAp) and the snail shell hydroxyapatite (SHAp) were studied using X-ray diffractometry. X-ray diffractometry (PANalytical, Empyrean) equipped with CuKα radiation (λ = 1.5406 Å) was used to identify the phase composition. Fourier transform infrared (FTIR) spectroscopy was used to ascertain the structure (functional groups) of CHAp and SHAp. The structure was complemented using Raman spectroscopy. FTIR (A Perkin Elmer) spectrometer integrated with Universal Attenuated Reflectance (UATR) sensor Two was used to obtain the infrared data on CHAp and SHAp over the range of 400 – 4000 cm^{-1}.

Raman spectroscopy (uRaman micro spectrometer) integrated with Nikon H550L upright microscope running on a uSoft 2.0 Map software for analysis. Using an x50 objective lens, the image of a field of the sample was captured. A laser beam of a wavelength 530.48 nm with a laser power of 100 mW was applied across the focused field at an integration time of 1500 ms to obtain a Raman spectrum of CHAp and SHAp.

3.3.3 Development of sensing platforms for cell studies

A volume of 0.5, 1.0, 2.0, 10.0, and 20% concentrations of CHAp and SHAp were prepared in double-distilled water using a downgrading serial dilution method (See Appendix A for the preparation method). The same volume of CHAp and SHAp of PEDOT-PSS polymers were added to the composition to increase adhesion between the HAp materials and the SPCEs.

A sensing platform was developed using SHAp/PEDOT: PSS blend to modify the SPCEs. The blend material (SHAp/PEDOT: PSS) was selected for the sensing platform also because of the high electrical conductivity and low impedance properties of PEDOT: PSS.

A volume of 2 µL of the CHAp and SHAp in the PEDOT: PSS mixture were pipetted and dropped to coat the working electrode area of the screen-printed carbon electrodes (SPCEs). The modified SPCEs were allowed to dry by heating at a temperature of 70˚C for 30 min on a hot plate. Figure 6 shows pictures of un-modified (A) and modified (B) SPCEs.

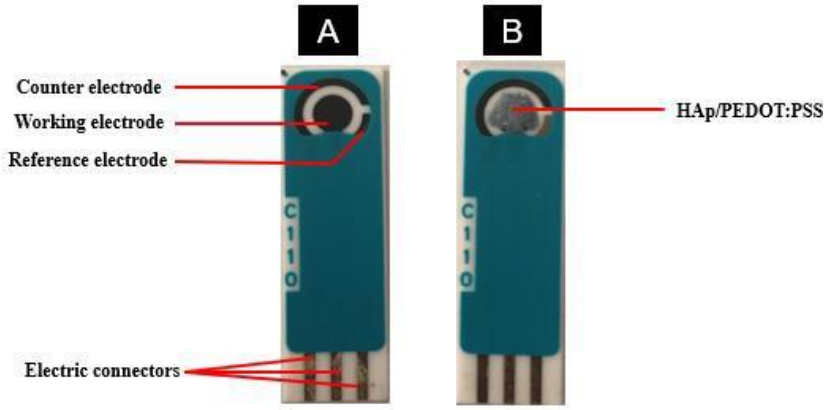

Figure 7 Pictures of SPCEs (A) unmodified SPCE showing counter electrode, working electrode, a reference electrode, and electric connectors (B) modified SPCE with HAp/PEDOT: PSS.

3.3.4 Cell culturing and cell seeding on modified SPCEs

Cell lines (human embryonic kidney transfection (HEK-293T) and pheochromocytoma (PC-12)) were cultured for seeding on modified screen-printed electrodes (SPCEs) alongside normal red blood cell (RBC) as control. HEK-293T was grown in DMEM media supplemented with fetal bovine serum (FBS), penicillin, streptomycin, and L-glutamine, whereas PC-12 was in RPMI 1640 media. All cell-lines were cultured at an incubation environment of 37°C with 5% CO_2. The cells were resuspended in their growth media and counted using trypan blue to stain the cells with a dilution factor of 1:10. Cell counts were performed using a hemocytometer, a counter, and a light microscope. The RBCs were suspended in phosphate-buffered saline of pH ~ 7.4. The cells, including the RBCs were centrifuged at 350 g for 5 min to get the cells forming a pellet. Cell counts of 4.17 x 10^7 cells/mL and 4 x 10^6 cells/mL and were obtained for cell-lines (HEK-293T and PC-12, respectively). The RBC concentration was also estimated at 4.10 x 10^7 cells /ml in PBS.

A volume of 5µL of the various cell pellets was pipetted and seeded onto the modified working electrode area of the SPCEs. Cell modified SPCE surfaces were incubated in a humid environment at 37°C for 30 min. SPCE surfaces were washed off gently with double distilled water to get rid of the excess unbound cells before electrochemical investigations proceeded.

3.3.5 Electrochemical measurements of modified and cell seeded modified SPCEs

A volume of 5 mM concentration of ferrocyanide solution containing 0.01M KCl in phosphate-buffered saline (PBS, pH 7.4) was prepared to use as an electrolyte for the electrochemical measurements (cyclic voltammetry and impedance spectroscopy) of the unmodified, modified and the cell-seeded modified screen-printed carbon electrodes (SPCEs). The electrochemical measurements were performed using an Autolab analyzer illustrated in Figure 8.

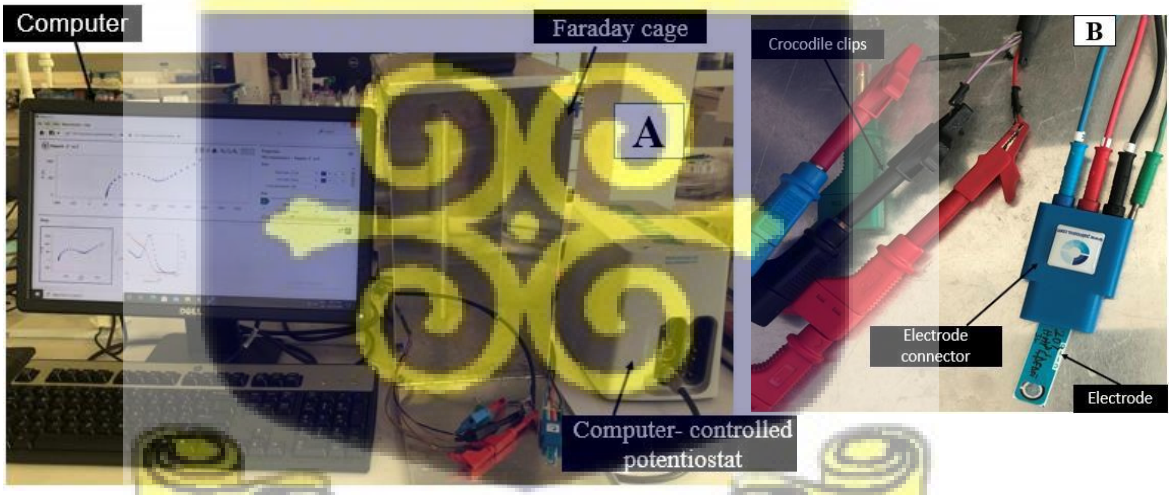

Figure 8 A picture of electrochemical analyser showing (A) the electrochemical analytical setup running on NOVA 2.1 software for the study (B) electrode setup connection parts.

Cyclic voltammograms of unmodified and modified SPCEs of various concentrations of CHAp and SHAp at 650, 750, and 850°C were recorded at applied potential range of -0.3 to + 0.6 V. A-scan rate study of 10 to 300 mV/s was run as shown in Table 1 in Appendix B and scan rate of 100 mv/s at a step voltage of 2.4 mV was used for all CV measurements.

Electrochemical impedance spectroscopy (EIS) was carried out under an alternating current with an amplitude of 0.098v within a frequency range of 0.1 to 100 kHz. The procedure to determine the EIS amplitude value is presented in Appendix C. EIS of unmodified SPCEs, modified SPCEs and cell seeded modified SPCEs were recorded and presented on a Nyquist plot.

CHAPTER FOUR

RESULTS

4.1 Introduction

This chapter reports the result obtained from the commercial hydroxyapatite (CHAp) and snail shells hydroxyapatite (SHAp) structural and electrochemical characterization. The chapter also presents the electrochemical responses recorded on the interaction of cells with CHAp- and SHAp-modified screen-printed carbon electrodes (SPCEs).

4.2 CHAp and SHAp characterization

X-ray diffractometry (XRD) was performed to identify the phase composition of the material. Figure 9 shows the XRD patterns of commercial hydroxyapatite (CHAp) and snail shells hydroxyapatite (SHAp). The XRD pattern of CHAp shows phases of only hydroxyapatite, whereas that of SHAp shows phases of hydroxyapatite and calcite. Fourier transform infrared (FTIR) analysis of the CHAp and SHAp material was performed to identify the material signature peaks (functional groups) and the characterization results are presented in Figure 10. CHAp and SHAp had characteristic vibrational PO_4^{3-} , CO^{2+}, and OH^- functional groups at wavenumber 1073, 1440, and 3573 cm^{-1}, respectively indicating that the materials are hydroxyapatite (HAp) (Asimeng, et al., 2018) (Ślósarczyk, Paszkiewicz, & Paluszkiewicz, 2005). The low OH^- transmission peak of SHAp suggests that SHAp is a Type B carbonated HAp material more than CHAp (Asimeng, et al., 2020). Figure 11 shows the Raman spectra of CHAp and SHAp. The CHAp and SHAp showed signature peaks of B-Type CO_3^{2-} functional

groups occurring at wavenumber (Raman shifts) 1124 cm^{-1}. The high Raman peak intensity of SHAp at 1124 cm^{-1} confirms the FTIR results that SHAp is more carbonated material than CHAp. The data from the FTIR and Raman analysis collaborates with data from the XRD analysis.

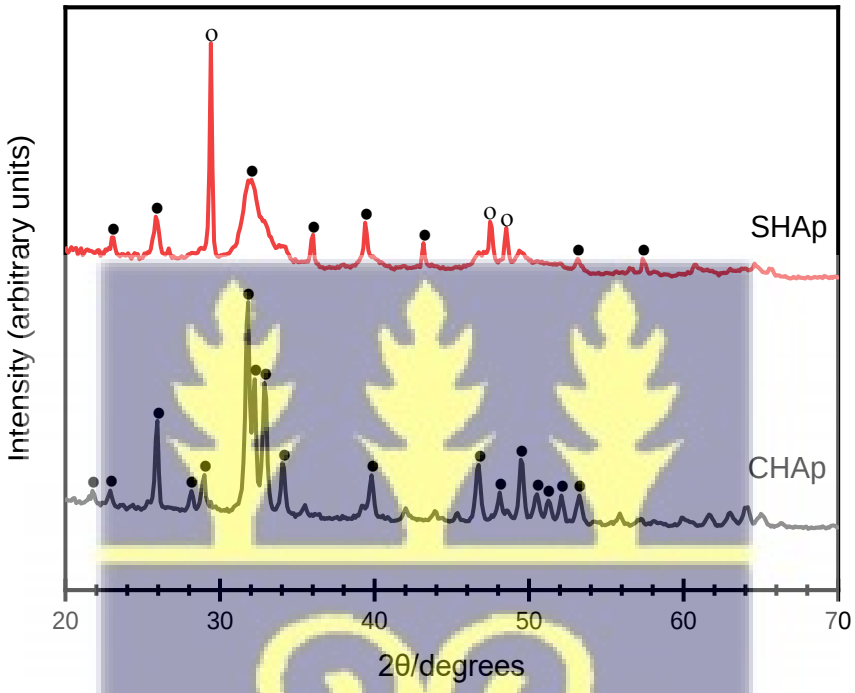

Figure 9 XRD patterns of CHAp and SHAp. The patterns indicate phases of hydroxyapatite (•) and calcite (o).

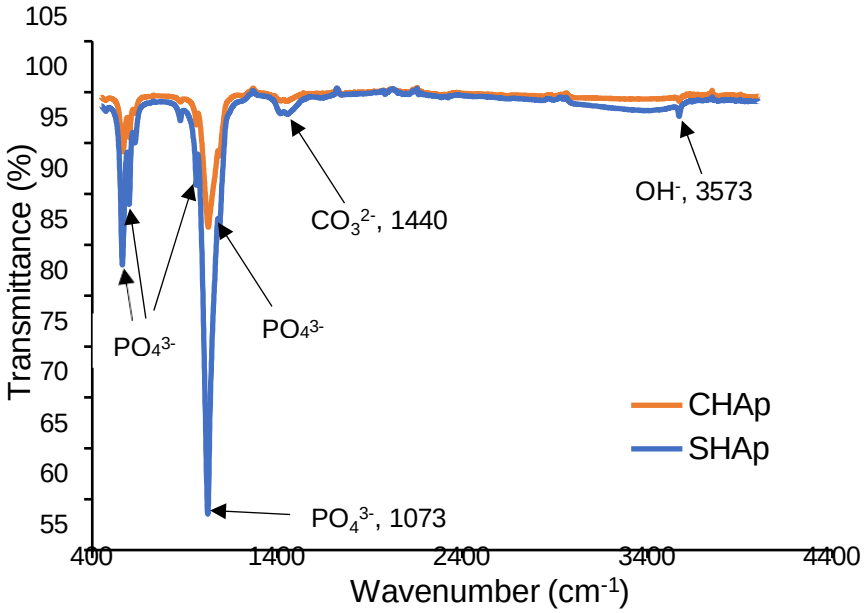

Figure 10 FTIR spectra of CHAp and SHAp in a wave range of 400cm^{-1} to 4000cm^{-1}

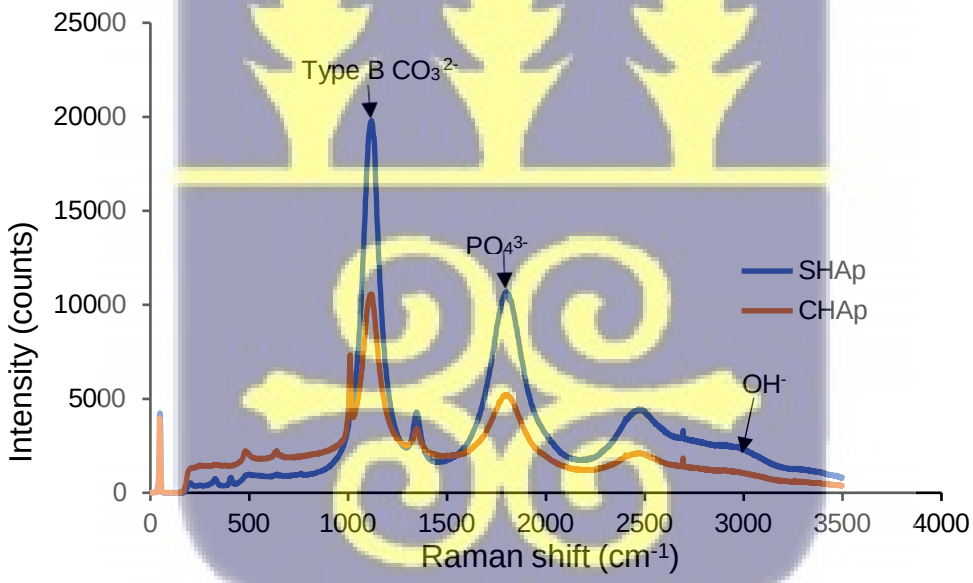

Figure 11 Raman spectra of CHAp and SHAp in a wave range of 0cm^{-1} to 3500cm^{-1}.

4.3 Electrochemical measurements

Figure 12 shows cyclic voltammograms obtained from the unmodified (bare) screen-printed carbon electrodes (SPCEs) in PBS (0.1M, pH 7.4) alone and in the presence of ferrocyanide. The SPCEs in PBS show no redox activity whereas the SPCEs show redox response in the presence of ferrocyanide with well-defined oxidation and reduction peaks occurring at potentials of 0.24 V and -0.004 V, respectively.

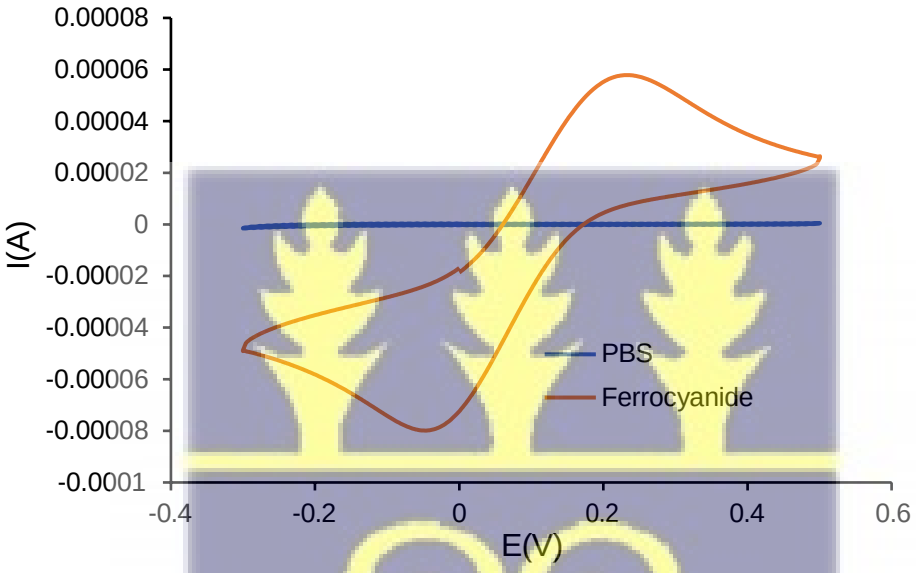

Figure 12 A cyclic voltammogram for SPCE in PBS and in 5 mM ferrocyanide containing 0.1M KCl. The voltammograms were obtained at a potential range of -0.3 to +0.5V (vs. Ag/AgCl) at a scan rate of 100 mv/s.

4.3.1 SPCEs modification with CHAp and SHAp materials

Figures 13 shows the cyclic voltammograms of SPCEs modified with commercial hydroxyapatite (CHAp) and snail shell hydroxyapatite (SHAp). It was observed in Figure 13 that there is a difference between CHAp and SHAp current responses in ferrocyanide

solution when compared to the unmodified SPCE. However, the SHAp shows high current response at the SPCE surface, so the SHap was compared to a conductive polymer (PEDOT: PSS) to study the influence of PEDOT: PSS on the current response of SHAp.

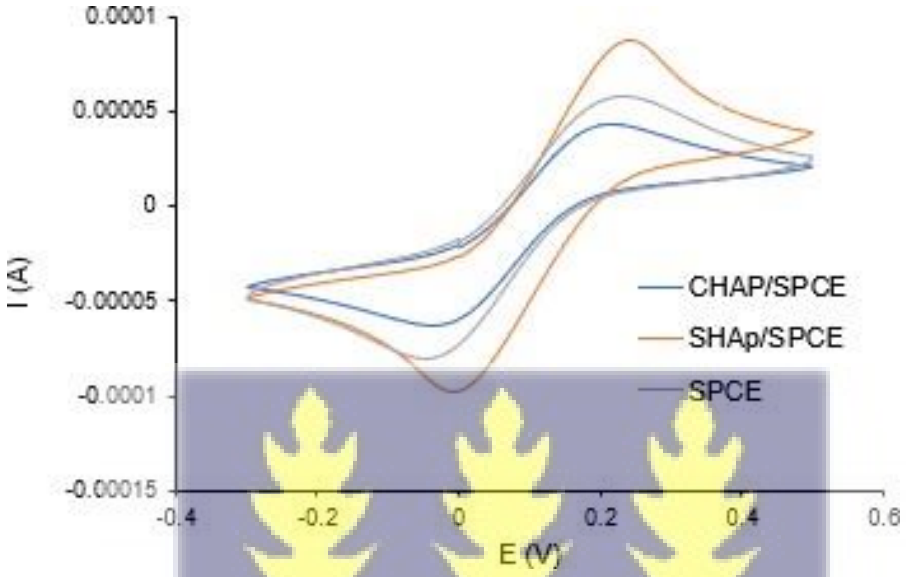

Figure 13 CVs of CHAp and SHAp with 5mM ferrocyanide containing 0.1M KCl. The voltammograms were obtained at a potential range of -0.3 to +0.5V (vs. Ag/AgCl) at a scan rate of 100 mv/s

Figure 14 shows the voltammograms of SHAp, PEDOT: PSS and SHAp/PEDOT: PSS blend. The PEDOT: PSS produced a significant current response of 247 µA which is about three-fold higher than that of SHAp (86.8 µA). The SHAp/PEDOT: PSS produced a current response of 266 µA which is close to the current of the PEDOT: PSS alone.

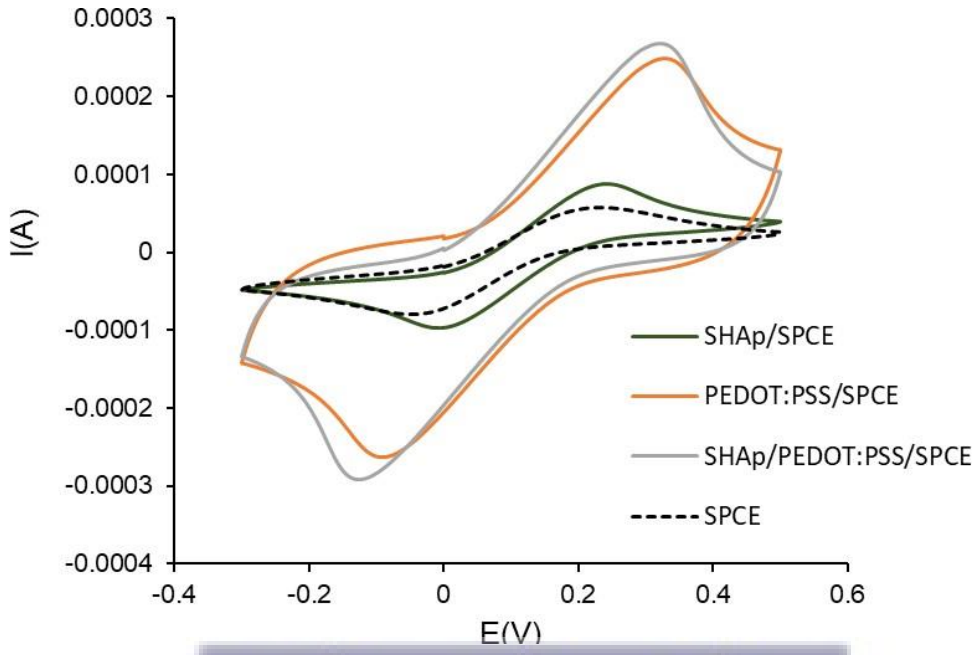

Figure 14 CV voltammograms of modified SHAp SPCE, PEDOT: PSS, and SHAp/PEDOT: PSS blend with 5 mM ferrocyanide containing 0.1M KCl. The voltammograms were obtained at a potential range of -0.3 to +0.5V (vs. Ag/AgCl) at a scan rate of 100 mv/s.

Electrochemical impedance spectroscopy (EIS) was performed to complement CV results in Figures 13 and 14. The EIS curve is presented in Figure 15 and 16 as Nyquist plots consisting of a semicircle section, located at higher frequencies corresponding to the electron transfer limited process. Its diameter represents the electron-transfer resistance or the charge transfer resistance (R_{CT}). The linear component of the Nyquist plot is related to the diffusion process held in solution and located at lower frequencies. The Nyquist plot in figure 15 shows the impedance (R_{CT}) produced by bare SPCE, CHAp (2.4 mΩ), and SHAp (1.64 mΩ) whereas Figure 16 shows R_{CT} of SHAp, PEDOT: PSS and SHAp/PEDOT: PSS.

It is noted that the semicircle diameter of the bare SPCE (1.2 mΩ) increased when both CHAp and SHAp were used to modify the SPCEs. The CHAp produced a higher R_{CT} value which is an indication of higher impedance and lower charge transfer (Figure 15). Figure 16 shows the R_{CT} of SHAp, PEDOT: PSS and SHAp/PEDOT: PSS blend. The PEDOT: PSS modified SPCE produced no R_{CT} value whereas SHAp modified SPCE produced an R_{CT} value of 1.64 mΩ. The introduction of PEDOT: PSS into SHAp (SHAp/PEDOT: PSS) reduced the R_{CT} value of SHAp modified SPCE to 0.25 mΩ.

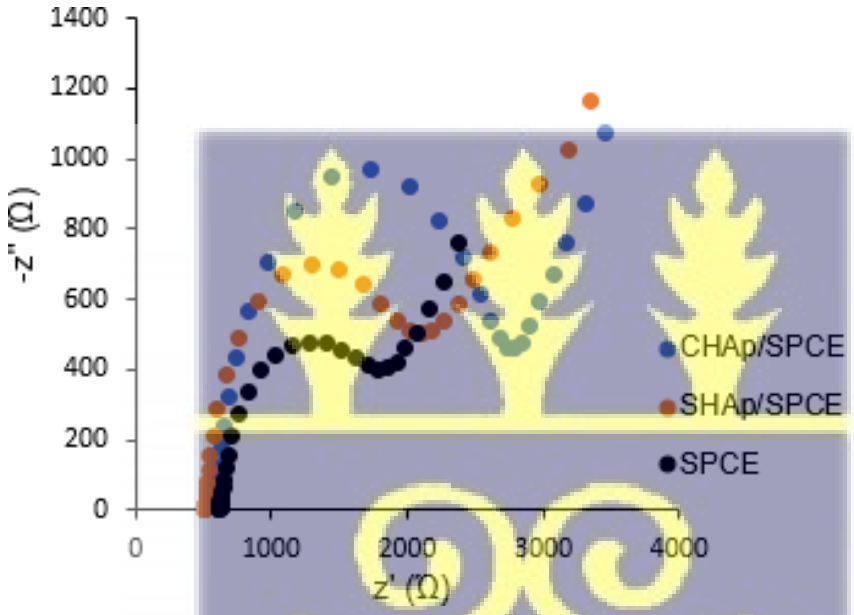

Figure 15 Nyquist plot of EIS results comparing the impedance of the SHAp and CHAp on the bare SPCE surface in 5mM ferrocyanide containing 01M KCl with an amplitude of 0.098 V within a frequency range of 0.1 to 100 kHz.

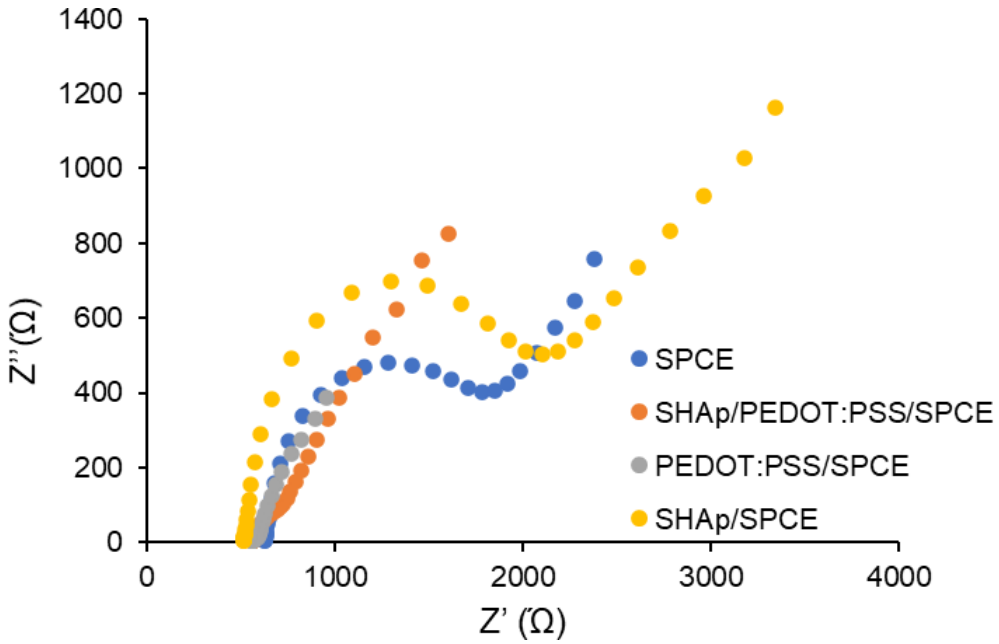

Figure 16 Nyquist plot showing EIS results of SHAp 850°C modified SPCE, PEDOT: PSS, and a nanocomposite of SHAp 850°C and PEDOT: PSS in 5mM ferrocyanide containing 0.1M KCl with an amplitude of 0.098 V within a frequency range of 0.1Hz to 100kHz.

4.3.1.1 Development of sensing SPCEs platform for cell studies

The cyclic voltammetry (CV) results in Figure 17 show that an increase in scan rates gave a corresponding increase in electrochemical current responses. The cathodic peaks shifted towards the positive potential while the anodic peaks shifted towards the negative potential. The Shifts in potential with increasing scan rates can be related to the internal resistance encountered inherently from the modified SPCE. The increase in current responses with increasing scan rate suggest that the kinetics of interfacial faradic redox reactions and the rate of electronic and ionic transport are increasing accordingly. The scan rate of 100 mV/s was selected for the cell studies because at 100 mV/s the Ip_a and Ip_c values are distinct from the scan rates below 100 mV/s. Upper scan rates above 100 mV/s

gave higher Ip_a and Ip_c values which is an advantage for the sensing platform, but the Ip_a and Ip_c values occur at a higher potential. The scan rate shows a linear correlation with anodic peak current (Ip_a) and cathodic peak current (Ip_c) as presented in Figure 18.

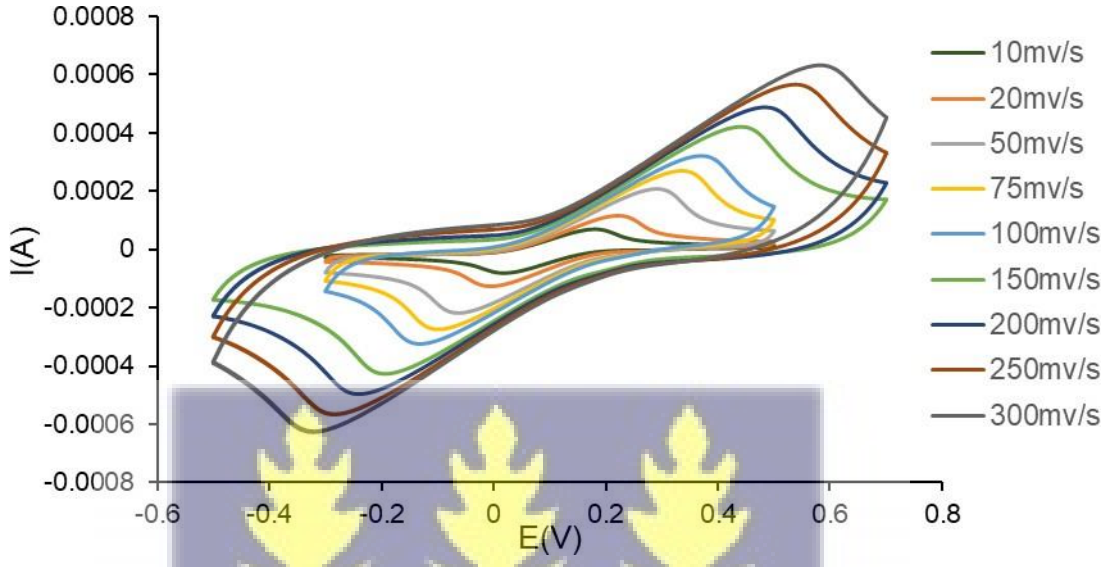

Figure 17 CVs of scan rates of SHAp/PEDOT: PSS on SPCE with a scan range of 10mv/s to 300mv/s. The experiment was conducted in 5mM ferrocyanide containing 0.1M KCl

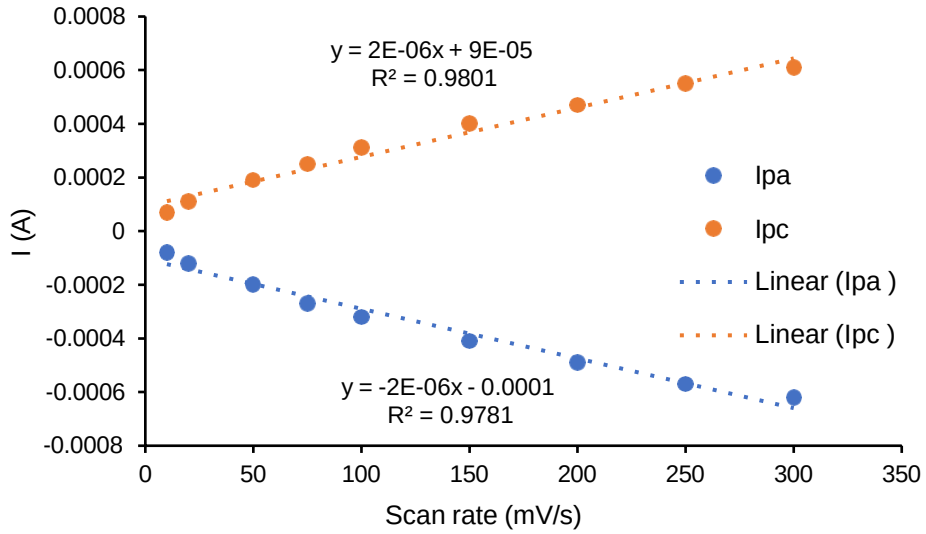

Figure 18 A graph of anodic (Ipa) and cathodic (Ipc) peak currents against scan rates. A linear correlation (R^2) was generated for both oxidation and reduction cycles.

4.3.2 Cell immobilization on SHAp/PEDOT: PSS modified SPCEs

Cell-lines (HEK-293T and PC-12) and normal cells (RBC) were immobilized on the SHAp/PEDOT: PSS modified SPCEs, and the CV and EIS results are presented in Figure 19 – 20. Figure 19 shows the peak current responses from RBC, HEK-293T, and PC- 12 after seeding on SHAp/PEDOT: PSS modified SPCEs. The RBC gave the highest peak current response of 230 µA, as compared to the cell-lines PC-12 (120 µA) and HEK- 293T (50 µA), respectively.

The EIS is presented as a Nyquist plot in Figure 20 which compares the impedance (Re) spectra of RBC, HEK-293T and PC-12 immobilized on the modified SPCEs and complements the CV results. The RBC recorded the least Re of 0.52 Ωm as compared to PC-12 (0.62 mΩ), and HEK-293T (0.70 mΩ), respectively.

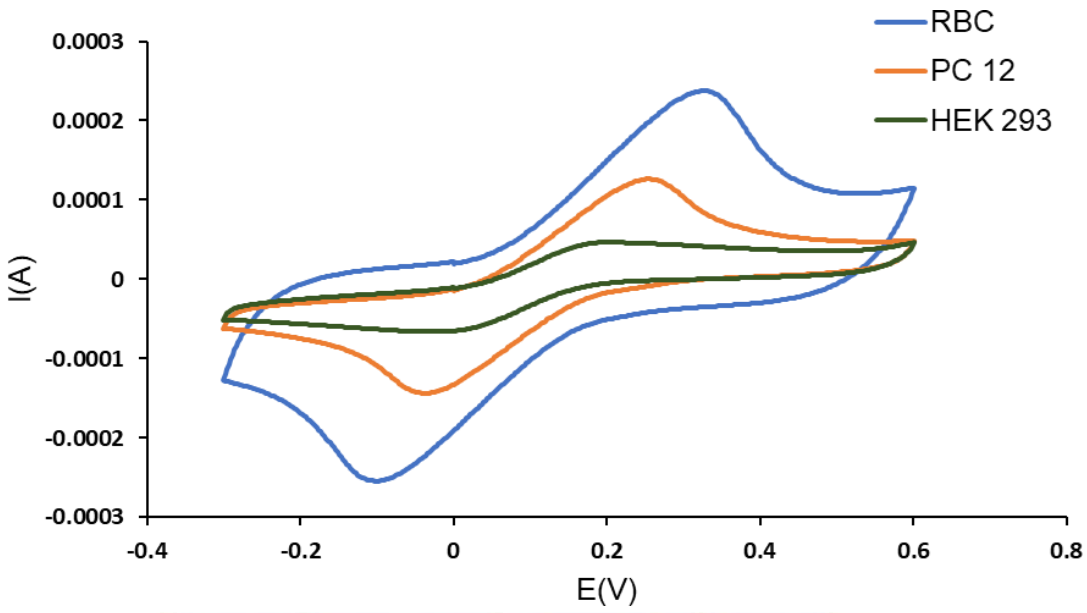

Figure 19 Cyclic voltammograms of RBC, PC 12, and HEK 293T cells immobilized on SHAp/PEDOT: PSS modified SPCE surface.

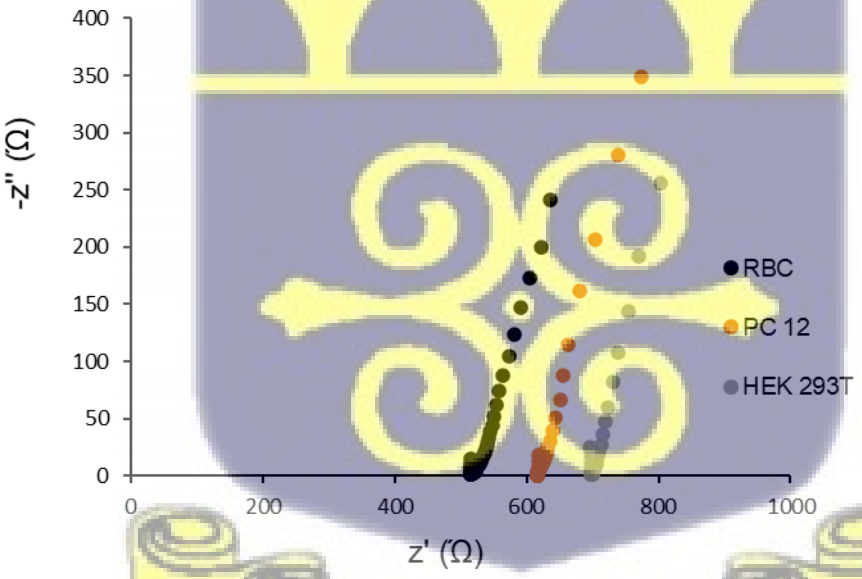

Figure 20 Nyquist plot of the impedance measure of RBC, PC 12, and HEK 293T in 5mM ferrocyanide containing 0.1M KCl with an amplitude of 0.098v within a frequency range of 0.1 to 100 kHz.

CHAPTER FIVE

DISCUSSION

The study aimed to investigate the use of hydroxyapatite (HAp) as an immobilizing material for label-free detection of cells. HAp was synthesized locally from *Achatina achatina* snail shells (SHAp) at 850ºC through a wet chemical precipitation method. Structural identification of the SHAp was performed alongside a commercially acquired hydroxyapatite (CHAp) using X-ray diffractometry (XRD), Fourier transform infrared (FTIR), and Raman spectroscopy. The XRD patterns of CHAp indicated only hydroxyapatite phases, which confirmed that the commercially acquired hydroxyapatite is pure hydroxyapatite. Also, hydroxyapatite and calcite phases present in the XRD pattern of SHAp confirmed that the synthesized material contained hydroxyapatite and calcite. CHAp and SHAp were further suggested to be hydroxyapatite molecules with the presence PO_4^{3-} , CO_3^{2-}, and OH^- functional groups. FTIR and Raman spectroscopy predict CHAp and SHAp were type B carbonate (CO_3^{2-}) substituted HAp, thus a replacement of PO_4^{3-} functional group with CO^{2-}, resulting in the low OH^- transmission peak in FTIR and a high-intensity peak in the Raman spectroscopy. Type B carbonate (CO_3^{2-}) substituted apatite is mostly found in biological sources of apatite (Asimeng, et al., 2020), (Asimeng, Karadag, Iftekhar, Xu, & Czernuszka, 2020), (Walters, Leung, Blumenthal, Konsker, & LeGeros, 1990). Figures 9 and 10 showed that the SHAp had higher intensities or concentrations of PO_4^{3-} , CO_3^{2-}, and OH^- functional groups present than the CHAp, thus SHAp was more carbonated than CHAp. The level and share of CO_3^{2-} substitution could be influenced by the source of HAp and the calcination temperature used. Snail shells naturally deposit carbonate materials in its shells due to its feeding habits, moreover the calcination temperature at 850ºC helps to decompose the organic waste for

purer calcite formation (Ooi, Hamdi, & Ramesh, 2007) (Asimeng, et al., 2018).

In this study, the inorganic compound, SHAp was exploited for the selective adsorption of cells in the development of a biosensor. Transducers in electrochemical biosensors transform a chemical reaction occurring on its surface from the biological elements into an electrical signal. This affords the necessary sensitivity to the sensor as signals produced must correlate directly to the signals measured. In this regard, electrodes in electrochemical biosensors should possess good signal transduction abilities. Screen-printed carbon electrodes (SPCE) were characterized as shown in Figure 12 to assess their performance and no peaks appeared for both the oxidative and reductive phases when cyclic voltammetry (CV) was run for SPCE in PBS. CV of SPCE with ferrocyanide produced peaks that inferred the validation of the suitability of using the carbon electrodes in the setup for electrochemical detections. Carbon-based electrodes have a wide potential window and a low background current making them preferable in the formation of screen-printed electrodes (SPE). SPEs come in a simple electrode setup and are cost-effective in mass production that allows its single usage for independent tests without contamination (Randviir, Brownson, Metters, Kadara, & Banks, 2014), (Krampa, Aniweh, Awandare, & Kanyong, 2017).

SHAp is a suitable interface at which redox reaction occurs because of the B-type carbonate substitution it underwent. The ionic diameter of carbonate is smaller than phosphate, so the replacement of the phosphate with carbonate allows SHAp to have a new structure conformation that makes SHAp more reactive than CHAp (Asimeng, et al., 2020). CV and electrochemical impedance spectroscopy (EIS) results in Figures 13 and 15, respectively suggest that SHAp is more conductive and introduces less impedance to the SPCE surface as compared to the CHAp. Due to the improved electrochemical responses of the SHAp, it was

selected as the suitable HAp material for SPCE modifications in the study.

For diagnostic purposes, a good biosensor should be able to produce sharp electrochemical responses, hence PEDOT: PSS a conductive polymer was introduced into SHAp to form a SHAp/PEDOT: PSS blend. The usage of blends that involves conductive polymers with other biomaterials has been widely used in biosensor fabrication and the formation tends to sharpen and increase the electrochemical responses. In addition, a conductive polymer blend enlarges the surface area of immobilizing materials in biosensors, and that makes it very sensitive and efficient (Krampa, Aniweh, Awandare, & Kanyong, 2017). A very drastic increase in peak current was observed when PEDOT: PSS was introduced into the SHAp indicating a sharp rise in conductivity as compared to the SHAp alone (Figure 14). This could be due to the synergetic increase in conductivity of the SHAp/PEDOT: PSS, thus a collaborative conductance from the SHAp and PEDOT: PSS, and the increase in the surface area of the blend formed. Impedance results in Figure 16 complement result in Figure 14 and show that the introduction of PEDOT: PSS drastically reduced the impedance produced by the SPCE inherently and the SHAp. The introduction of the conductive polymer into SHAp did not only increase its conductivity but also helped the SHAp to stick better on the electrode surface as compared to the SHAp alone for cell immobilization studies. The high R^2 values obtained for the anodic peak (Ip_a) and cathodic peak (Ip_c) currents of the fabricated SHAp/PEDOT: PSS modified SPCE for both the oxidation and reduction cycles (Figure 17), suggests that there is high consistency in current values when scan rate is increased, and this indicates that the electron flow mechanism of modified SPCEs was under a diffusion-controlled state. All this data provided shows that SHAp/PEDOT: PSS is a good immobilizing material for transducer modification especially carbon-based electrodes for sensor development as it allows for good signal transduction, removing all inherent impedance from the transducing surface, hence any

signal obtained is from the biorecognition element immobilized on the transducing surface.

Human cells, both pathogenic and non-pathogenic contain sialic acid, a carbon receptor molecule that can be found on the terminal regions of glycan chains on cell membranes. Sialic acid moieties have been associated with several diseases including cancer and find relevance in cell targeting. Sialic acid moieties are important in key activities including cellular signaling and proliferation, cell-to-cell adhesion and interaction, and host-to-pathogen interactions. HAp is known to have an adhesive interaction with sialic acid on cell surfaces although this phenomenon has not been exhaustively understood yet (Asimeng, et al., 2019) (Luukkonen, et al., 2019). Detection of cells through the interaction of sialic acid on cell surfaces and HAp can be used for label-free cancer cell detection. This would help in the reduction of interferences from normal cell activities, improvement in kinetic measurement, simplicity in assay formation, and a reduction in assay measurement time (Solly, Wang, Xu, Strulovici, & Zheng, 2004). Cell lines (human embryonic kidney transfection (HEK-293T) and pheochromocytoma (PC-12)) and normal cell (red blood cells (RBC)) were immobilized and the CV Figure 19 recorded a high current for RBC as compared to PC-12 and HEK-293T, respectively. The CV results were complemented by EIS results Figure 20 which further suggests that RBC recorded lower impedance values than PC-12 and HEK-293T. These results could be attributed to the difference in the electrical behavior of individual cells through polarization and depolarization mechanisms resulting in an ion-concentration gradient across their cell membranes. Normal human cells mostly undergo polarization by the efflux of ions from their cytoplasm to their outer environment to obtain a balanced resting potential thereby increasing their external ion concentration, whereas cancer cells mostly undergo depolarization through the influx of ions from their external environment into their cytoplasm thereby reducing ion concentration on its outer environment (Yang & Brackenbury, 2013), (Asimeng,

et al., 2019).

A decrease in impedance was recorded for all cells seeded on the modified SPCE (Figure 20) This contrasts with some studies that have employed EIS to probe surface changes after biorecognition element immobilizations (Gu & Zhao, 2010), (Jiang & Spencer, 2010), (Chowdhury, Ganganboina, Park, & Doong, 2018). It is important to note that, the SHAp/PEDOT: PSS modification results in an alteration of the surface structure of the SPCE. The SHAp/PEDOT: PSS blends are porous in structure, so cells can occupy the pores without direct attachment to the electrode surface. Although this speculation is not supported by imaging techniques in this study, there is growing evidence in literature (Yokogawa, Seelan, & Zhang, 2006), (Chowdhury, Ganganboina, Park, & Doong, 2018). This reason is attributed to the gradual decrease in R_{CT} values obtained. A proposed mechanism of the principle underlying the R_{CT} changes in this study compared to other studies is illustrated in figure 20.

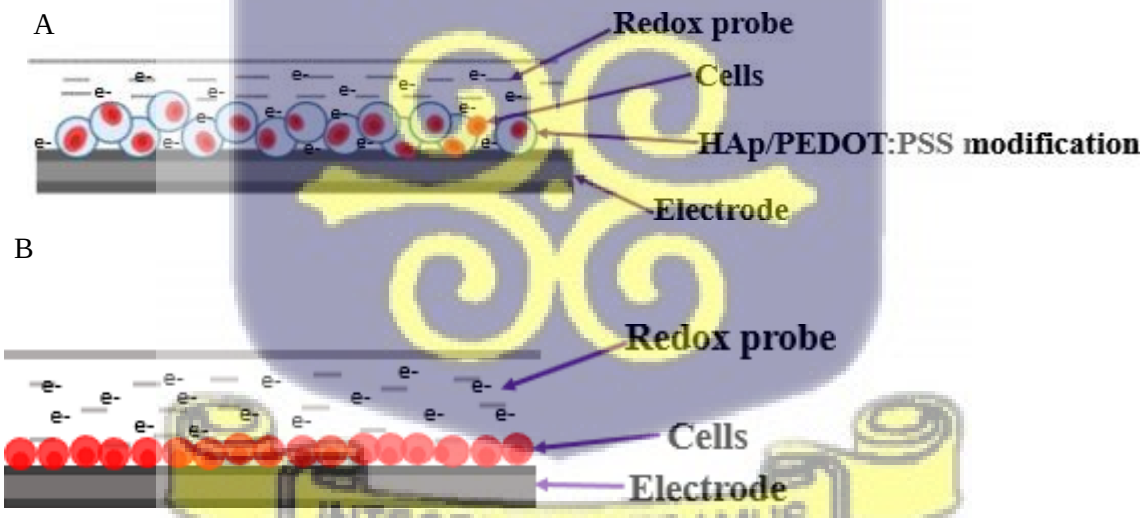

Figure 21 Diagrams showing the proposed mechanisms of cell capture in this study (A) SHAp/PEDOT: PSS modified electrode captures cells within its porous matrix in an electrolyte for electrochemical measurements, and other studies (B) cells directly attaching to electrode surfaces to insulate it.

CHAPTER SIX

CONCLUSION AND RECOMMENDATION

6.1 CONCLUSION

In this study, the immobilization of normal red blood cells (RBC) and cell lines, human embryonic kidney transfection (HEK-293T), and pheochromocytoma (PC-12) using a hydroxyapatite material synthesized from *Achatina achatina* snail shells (SHAp) for the fabrication of a cell-based biosensor are investigated. SHAp recorded good electrochemical responses suitable for use as an immobilizing material for electrochemical cytosensing. SHAp was mixed with PEDOT: PSS, a conductive polymer to form a SHAp/PEDOT: PSS blend for the modification of the screen-printed carbon electrode (SPCE). Scan rate analysis on the modified SPCE recorded a linear correlation of 0.98 which suggests that the SHAp/PEDOT: PSS on the SPCE is suitable to be used as a transducing surface for electrochemical biosensing. Cyclic voltammetry (CV) and electrochemical impedance spectroscopy (EIS) measurements were performed to record the cell proliferation signals. The CV results showed low peak currents (50 and 120 µA) for HEK-293T and PC-12, respectively, whereas a high peak current (230 µA) for control RBC. The EIS showed impedance values of 0.70 and 0.62 mΩ for HEK-293T and PC-12 respectively, and 0.52 mΩ for RBC. The findings demonstrate that SHAp can differentiate between the proliferation signals of cells through potentiometric and impedimetric measurements. The unique current difference among the cells could be used as potential markers for the differentiation of cells.

6.2 RECOMMENDATION

In recognition of the increase in conductivity of hydroxyapatite synthesized from *Achatina achatina* snail shells (SHAp) at 850ºC, future studies regarding the application of the SHAp should consider its synthesis cat higher temperatures. This will help determine the most appropriate temperature which enables its use in electrochemical sensing and its relation to the biocompatibility of cells. Moreover, due to the electroactive nature of SHAp shown in this study, it is recommended for integration into other useful sensing areas such as chemosensing.

This study demonstrated the use of SHAp for label-free cell detection in electrochemical systems without the use of additional reagents, suggesting the possibility of rapid self-contained sensing systems for cancer cell detection. Considering that, screen-printed carbon electrodes enable miniaturization of such platforms, a combination of printed electrodes in conjunction with composites and label-free assay strategies represent a perfect biosensing system. Furthermore, microelectrodes can also be considered as it provides a better-miniaturized device with less background current and potential.

However, the speculations made in cell capture require further investigations such as electrochemical standardizations and the use of imaging techniques to establish definitive conclusions.

REFERENCE

Altintas, Z., & Tothill, I. (2013). *Biomarkers and biosensors for the early diagnosis of lung cancer*. *Sensors and Actuators B: Chemica*, 188, 988-998.

Altintas, Z., Uludag, Y., Gurbuz, Y., & Tothill, I. (2012). *Development of surface chemistry for surface plasmon resonance-based sensors for the detection of proteins and DNA molecules*. *Analytica chimica acta*, 712, 138-144.

Altintas, Z., Uludag, Y., Gurbuz, Y., & Tothill, I. E. (2011). *Surface plasmon resonance based immunosensor for the detection of the cancer biomarker carcinoembryonic antigen*. *Talanta*, 86, 377-383.

Anderson, D. E., Balapangu, S., Fleischer, H. N., Viade, R. A., Krampa, F. D., Kanyong, P., & Tiburu, E. K. (2017). Investigating the influence of temperature on the kaolinite-base synthesis of zeolite and urease immobilization for the potential fabrication of electrochemical urea biosensors. *sensors*, 17(8), 1831.

Are, C., Rajaram, S., Are, M., Raj, H., Anderson, B. O., Chaluvarya Swamy, R., & Cazap, E. L. (2013). A review of global cancer burden: trends, challenges, strategies, and a role for surgeons. *Journal of surgical oncology*, 107(2), 221-226.

Asimeng, B. O., Fianko, J. R., Kaufmann, E. E., Tiburu, E. K., Hayford, C. F., Anani, P. A., & Dzikunu, O. K. (2018). Preparation and characterization of hydroxyapatite from A chatina achatina snail shells: effect of carbonate substitution and trace elements on defluoridation of water. *Journal of Asian Ceramic Societies*, 6(3), 205-212.

Asimeng, B. O., Karadag, I., Iftekhar, S., Xu, Y., & Czernuszka, J. (2020). XRD and IR revelation of a unique gC 3 N 4 phase with effects on collagen/hydroxyapatite bone scaffold pore geometry and stiffness. *SN Applied Sciences*, 2(8), 1-10.

Asimeng, B. O., Tiburu, E. K., Effah Kaufmann, E., Paemka, L., Hayford, C. F., Essien-Baidoo, S., & Anani, P. A. (2019). Electrochemical evaluation of ion substituted-hydroxyapatite on HeLa cells plasma membrane potential. *Cogent Engineering*, 6(1), 16.

Asimeng, B. O., Tiburu, E. K., Kan-Dapaah, K., Efavi, J. K., Asiamah, R., & Afeke, D. W. (2020). Influence of preferred orientation on the bioactivity of hydroxyapatite: a potential tooth repair and implant surface coating material. *Cerâmica*, 66(379), 340.

Asphahani, F., & Zhang, M. (2007). Cellular impedance biosensors for drug screening and toxin detection. *Analyst*, 132(9), 835-841.

Bahadır, E. B., & Sezgintürk, M. K. (2016). A review on impedimetric biosensors. *Artificial cells, nanomedicine, and biotechnology*, 44(1), 248-262.

Bajaj, A., Miranda, O. R., Kim, I. B., Phillips, L., R., Jerry, D. J., . . . Rotello, V. M. (2009). Detection and differentiation of normal, cancerous, and metastatic cells using nanoparticle-polymer sensor arrays. *Proceedings of the National Academy of Sciences*, 106(27), 10912-10916.

Banerjee, P., & Bhunia, A. K. (2009). Mammalian cell-based biosensors for pathogens and toxins. *Trends in biotechnology*, 27(3), 179-188.

Barnard, K. N., Wasik, B. R., LaClair, J. R., Buchholz, D. W., Weichert, W. S., Alford-Lawrence, B. K., & Parrish, C. R. (2019). Expression of 9-O-and 7, 9-O-acetyl modified sialic acid in cells and their effects on influenza viruses. *mBio*, 10(6).

Bharath, G. M., Chen, S. M., Veeramani, V., Balamurugan, A., Mangalaraj, D., & Ponpandian, N. (2015). Enzymatic electrochemical glucose biosensors by mesoporous 1D hydroxyapatite-on-2D reduced graphene oxide. . *Journal of Materials Chemistry*, 3(7), 1360-1370.

Blackadar, C. B. (2016). Historical review of the causes of cancer. *World journal of clinical oncology*, 7(1), 54.

Bohunicky, B., & Mousa, S. A. (2011). Biosensors: the new wave in cancer diagnosis. *Nanotechnology, science and applications*, 4, 1.

Bumbrah, G. S., & Sharma, R. M. (2016). Raman spectroscopy–Basic principle, instrumentation and selected applications for the characterization of drugs of abuse. *Egyptian Journal of Forensic Sciences*, 6(3), 209-215.

Canbaz, M. Ç., & Sezgintürk, M. K. (2014). Fabrication of a highly sensitive disposable immunosensor based on indium tin oxide substrates for cancer biomarker detection. *Analytical biochemistry*, 446, 9-18.

Carpelan-Holmström, M., Louhimo, J., Stenman, U. H., Alfthan, H., & Haglund, C. C. (2002). CEA, CA 19-9 and CA 72-4 improve the diagnostic accuracy in gastrointestinal cancers. *Anticancer research*, 22(4), 2311-2316.

Chatterjee, S. K., & Zetter, B. R. (2005). Cancer biomarkers: knowing the present and predicting the future.

Chikkaveeraiah, B. V., Bhirde, A. A., Morgan, N. Y., Eden, H. S., & Chen, X. (2012). Electrochemical immunosensors for detection of cancer protein biomarkers. *ACS nano*, 6(8), 6546-6561.

Chowdhury, A. D., Ganganboina, A. B., Park, E. Y., & Doong, R. A. (2018). Impedimetric biosensor for detection of cancer cells employing carbohydrate targeting ability of Concanavalin A. *Biosensors and Bioelectronics*, 122, 95-103.

Cox, J. N. (1992). Fourier transform infrared spectroscopy. *Encyclopedia of Materials Characterization-Surfaces, Interfaces, Thin Films*, 416-427.

Del Sol, A., Balling, R., Hood, L., & Galas, D. (2010). Diseases as network perturbations. *Current opinion in biotechnology*, 21(4), 566-571.

Ding, C., Li, X., Wang, W., & Chen, Y. (2016). Fluorescence detection of telomerase activity in cancer cell extracts based on autonomous exonuclease III-assisted isothermal cycling signal amplification. *Biosensors and Bioelectronics*, 83, 102-105.

Dorledo de Faria, R. A., Iden, H., Heneine, L. G., Matencio, T., & Messaddeq, Y. (2019). Non-enzymatic impedimetric sensor based on 3-Aminophenylboronic acid functionalized screen-printed carbon electrode for highly sensitive glucose detection. . *Sensors*, 19(7), 1686.

D'Souza, T., Agarwal, R., & Morin, P. J. (2005). Phosphorylation of claudin-3 at threonine 192 by cAMP-dependent protein kinase regulates tight junction barrier function in ovarian cancer cells. *Journal of Biological Chemistry*, 280(28), 26233-26240.

Fan, G., Lu, W., Wang, X., & Liang, F. (2008). Phase transition behaviour and electromechanical properties of (Na1/2Bi1/2) TiO3–KNbO3 lead-free piezoelectric ceramics. *Journal of Physics D: Applied Physics*, 41(3), 035403.

Farzin, L., Shamsipur, M., Samandari, L., & Sheibani, S. (2018). Signalling probe displacement electrochemical aptasensor for malignant cell surface nucleolin as a breast cancer biomarker based on gold nanoparticle decorated hydroxyapatite nanorods and silver nanoparticle labels. . *Microchimica Acta*, 185(2), 154.

Ferlay, J., Colombet, M., Soerjomataram, Mathers, C., Parkin, D., Piñeros, M., . . . Bray, F. (2019). Estimating the global cancer incidence and mortality in 2018: *International Journal of Cancer*.

Futreal, P. A., Coin, L., Marshall, M., Down, T., Hubbard, T., Wooster, R., & Stratton, M. R. (2004). A census of human cancer genes. *Nature reviews cancer*, 4(3), 177-183.

Gómez-Morales, J., Iafisco, M., Delgado-López, J. M., Sarda, S., & Drouet, C. (2013). Progress on the preparation of nanocrystalline apatites and surface characterization: Overview of fundamental and applied aspects. . *Progress in Crystal Growth and Characterization of Materials*, 59(1), 1-46.

Gong, T., Cui, Y., Goh, D., Voon, K. K., Shum, P. P., Humbert, G., & & Olivo, M. (2015). Highly sensitive SERS detection and quantification of sialic acid on single cell

using photonic-crystal fiber with gold nanoparticles. *Biosensors and Bioelectronics*, 64, 227-233.

Gu, W., & Zhao, Y. (2010). Cellular electrical impedance spectroscopy: an emerging technology of microscale biosensors. *Expert review of medical devices*, 7(6), 767-779.

Hayakawa, T. N., Ishiguro, H., Kondo, T., Kurimoto, K., & Noda, A. (1999). A prospective multicenter trial evaluating diagnostic validity of multivariate analysis and individual serum marker in differential diagnosis of pancreatic diseases. *International journal of pancreatology*, 25(1), 23-29.

Hoerger, T. J., Ekwueme, D. U., Miller, J. W., Uzunangelov, V., Hall, I. J., Segel, J., & Li, C. (2011). Estimated effects of the National Breast and Cervical Cancer Early Detection Program on breast cancer mortality. *American journal of preventive medicine*, 40(4), 397-404.

Huls, N. F., Phan, M. H., Kumar, A., Mohapatra, S., Mohapatra, S., Mukherjee, P., & Srikanth, H. (2013). Transverse susceptibility as a biosensor for detection of Au-Fe3O4 nanoparticle-embedded human embryonic kidney cells. *Sensors*, 13(7), 8490-8500.

Jayanthi, V. S., Das, A. B., & Saxena, U. (2017). *Recent advances in biosensor development for the detection of cancer biomarkers*. *Biosensors and Bioelectronics*, 91, 15-23.

Jerónimo, P. C., Araújo, A. N., & Montenegro, M. C. (2007). Optical sensors and biosensors based on sol–gel films. *Talanta*, 72(1), 13-27.

Jiang, X., & Spencer, M. G. (2010). Electrochemical impedance biosensor with electrode pixels for precise counting of CD4+ cells: A microchip for quantitative diagnosis of HIV infection status of AIDS patients. *Biosensors and Bioelectronics*, 25(7), 1622-1.

Jianrong, C., Yuqing, M., Nongyue, H., Xiaohua, W., & Sijiao, L. (2004). Nanotechnology and biosensors. *Biotechnology advances*, 22(7), 505-518.

Kesharwani, P., Mishra, V., & Jain, N. K. (2015). Validating the anticancer potential of carbon nanotube-based therapeutics through cell line testing. *Drug discovery today*, 20(9), 1049-1060.

Kim, H. I., Lim, H., & Moon, A. (2018). Sex differences in cancer: epidemiology, genetics and therapy. *Biomolecules & therapeutics*, 26(4), 335.

Koschwanez, H. E., & Reichert, W. M. (2007). In vitro, in vivo and post explantation testing of glucose-detecting biosensors: current methods and recommendations. *Biomaterials*, 28(25), 3687-3703.

Krampa, F. D., Aniweh, Y., Awandare, G. A., & Kanyong, P. (2017). A disposable amperometric sensor based on high-performance PEDOT: PSS/ionic liquid nanocomposite thin film-modified screen-printed electrode for the analysis of catechol in natural water samples. *Sensors*, 17(8), 1716.

Kumar, S., Mohan, A., & Guleria, R. (2006). Biomarkers in cancer screening, research and detection: present and future: a review. *Biomarkers*, 11(5), 385-405.

Lin, K. &. (2015). Structure and properties of hydroxyapatite for biomedical applications. In Hydroxyapatite (HAp) for biomedical applications. *Woodhead Publishing*, pp. 3-19.

Lingen, M. W., Kalmar, J. R., Karrison, T., & Speight, P. M. (2008). Critical evaluation of diagnostic aids for the detection of oral cancer. *Oral oncology*, 44(1), 10-22.

Lisdat, F., & Schäfer, D. (2008). The use of electrochemical impedance spectroscopy for biosensing. *Analytical and bioanalytical chemistry*, 391(5), 1555.

Liu, Q., Yu, J., Xiao, L., Tang, J. C., Zhang, Y., Wang, P., & Yang, M. (2009). Impedance studies of bio-behavior and chemosensitivity of cancer cells by micro-electrode arrays. *Biosensors and Bioelectronics*, 24(5), 1305-1310.

Lodish, H., Berk, A., Zipursky, S. L., Matsudaira, P., Baltimore, D., & Darnell, J. (2000). Muscle: A specialized contractile machine. *In Molecular Cell Biology*, 4th edition. WH Freeman.

Long, D. A. (2002). *The Raman effect: a unified treatment of the theory of Raman scattering by molecules.*

Luukkonen, J., Hilli, M., Nakamura, M., Ritamo, I., Valmu, L., Kauppinen, K., & Lehenkari, P. (2019). Osteoclasts secrete osteopontin into resorption lacunae during bone resorption. Histochemistry and cell biology, 151(6), 475-487.

Ma, G., & Liu, X. (2009). Hydroxyapatite: hexagonal or monoclinic. Cryst. Growth Des.

Ma, X., & Yu, H. (2006). Cancer issue: global burden of cancer. The Yale journal of biology and medicine, 79(3-4), 85.

Martland, H. S. (1931). The occurrence of malignancy in radio-active persons: A general review of data gathered in the study of the radium dial painters, with special reference to the occurrence of osteogenic sarcoma and the inter-relationship of certain. The American Journal of Cancer, , 15(4), 2435-2516.

Mehdi, M. M., Singh, P., & Rizvi, S. I. (2012). Erythrocyte sialic acid content during aging in humans: correlation with markers of oxidative stress. Disease markers, 32(3), 179-186.

Molassiotis, A., Wilson, B., Brunton, L., & Chandler, C. (2010). Mapping patients' experiences from initial change in health to cancer diagnosis: a qualitative exploration of patient and system factors mediating this process. European journal of cancer care, 19(1), 98-109.

Murakami, L. M., Diniz, M. F., Silva, L. M., Sanches, N. B., & Dutra, R. D. (2019). Off-line TLC-IR (UATR) characterization of additives in EPDM rubber. Polymer Testing, 79, 106042.

Murugan, R., & Ramakrishna, S. (2005). Crystallographic study of hydroxyapatite bioceramics derived from various sources. *Crystal Growth & Design*, 5(1), 111-112.

Naseri, M., Fotouhi, L., & Ehsani, A. (2018). Recent Progress in the Development of Conducting Polymer-Based Nanocomposites for Electrochemical Biosensors Applications: A Mini-Review. *The Chemical Record*, 18(6), 599-618.

Nolan, J. P., Duggan, E., Liu, E., Condello, D., Dave, I., & Stoner, S. A. (2012). *Single cell analysis using surface enhanced Raman scattering (SERS) tags.* Methods, 57(3), 272-279.

Ooi, C. Y., Hamdi, M., & Ramesh, S. (2007). Properties of hydroxyapatite produced by annealing of bovine bone. Ceramics international, 33(7), 1171-1177.

Ouyang, L., Hu, Y., Zhu, L., Cheng, G. J., & Irudayaraj, J. (2017). A reusable laser wrapped graphene-Ag array-based SERS sensor for trace detection of genomic DNA methylation. *Biosensors and Bioelectronics*, 92, 755-762.

Pang, X. Z. (2005). Electrodeposition of composite hydroxyapatite–chitosan films. *Materials Chemistry and Physics*, 94(2-3), 245-251.

Parkin, D. M., Bray, F., Ferlay, J., & Pisani, P. (2005). Global cancer statistics, 2002. *A cancer journal for clinicians*, 55(2), 74-108.

Porter, C. A., & White, C. J. (1907). Multiple Carcinomata following Chronic X-ray Dermatitis. *Annals of surgery*, 46(5), 649.

Poste, G., Carbone, D. P., Parkinson, D. R., Verweij, J., Hewitt, S. M., & Jessup, J. M. (2012). Leveling the playing field: bringing development of biomarkers and molecular diagnostics up to the standards for drug development.

Putzbach, W., & Ronkainen, N. J. (2013). Immobilization techniques in the fabrication of nanomaterial-based electrochemical biosensors: A review. *Sensors*, 13(4), 4811-4840.

Qi, P., Wan, Y., & Zhang, D. (2013). Impedimetric biosensor based on cell-mediated bioimprinted films for bacterial detection. *Biosensors and Bioelectronics*, 39(1), 282-288.

Randviir, E. P., Brownson, D. A., Metters, J. P., Kadara, R. O., & Banks, C. E. (2014). The fabrication, characterisation and electrochemical investigation of screen-printed graphene electrodes. *Physical Chemistry Chemical Physics*, 16(10), 4598-4611.

RL, S., KD, M., & A, J. (2017 jan). Cancer Statistics, 2017. *CA Cancer J Clin.* , 67(1):7-30.

Rusling, J. F., Kumar, C. V., Gutkind, J. S., & Patel, V. (2010). Measurement of biomarker proteins for point-of-care early detection and monitoring of cancer. *Analyst*, 135(10)2496-2511.

S.K., V., L.G., D., S., B., & J.H., L. (2019). Future Trends for the Next Generation of Personalized and Integrated Healthcare for Chronic Diseases. InPoint-of-Care Technologies Enabling Next-Generation Healthcare Monitoring and Management. *Springer*, pp. 209-223.

Sadikovic, B., Al-Romaih, K., Squire, J. A., & Zielenska, M. (2008). Cause and consequences of genetic and epigenetic alterations in human cancer. *Current genomics*, 9(6), 394-408.

Schiffman, J. D., Fisher, P. G., & Gibbs, P. (2015). Early detection of cancer: past, present, and future. *American Society of Clinical Oncology Educational Book*, 35(1), 57-65.

Scholz, F. (2010). Thermodynamics of electrochemical reactions. In Electroanalytical Methods. *Springer, Berlin, Heidelberg*, pp. 11-31.

Sheng, G., Xu, G., Xu, S., Wang, S., & Luo, X. (2015). Cost-effective preparation and sensing application of conducting polymer PEDOT/ionic liquid nanocomposite with excellent electrochemical properties. . *Royal Society of Chemistry*, 5(27), 20741-20746.

Siegal, R., Miller, K. D., & Jemal, A. (2014). Cancer statistics, 2012. *Ca cancer J clin*, 64(1), 9-29.

Siegel, R. L., Miller, K. D., & A., J. (2017). Cancer statistics, 2017. *CA Cancer J Clin*, 67(1), 7-30.

SK, V., LG, D., S, B., & JH., L. (2019). Future Trends for the Next Generation of Personalized and Integrated Healthcare for Chronic Diseases. InPoint-of-Care Technologies Enabling Next-Generation Healthcare Monitoring and Management . *springer, cham*, pp. 209-223.

Skoog, D. A., Holler, F. J., & Crouch, S. R. (2017). Principles of instrumental analysis. *Cengage learning*.

Ślósarczyk, A., Paszkiewicz, Z., & Paluszkiewicz, C. (2005). FTIR and XRD evaluation of carbonated hydroxyapatite powders synthesized by wet methods. *Journal of Molecular Structure*, 744, 657-661.

Solly, K., Wang, X., Xu, X., Strulovici, B., & Zheng, W. (2004). Application of real-time cell electronic sensing (RT-CES) technology to cell-based assays. *Assay and drug development technologies*, 2(4), 363-372.

Tanaka, Y., Kikuchi, M., Tanaka, K., Hashimoto, K., Hojo, J., Nakamura, M., & Yamashita, K. (2010). Fast oxide ion conduction due to carbonate substitution in hydroxyapatite. *Journal of the American Ceramic Society*, 93(11), 3577-3579.

Thévenot, D., Toth, K., Durst, R., & Wilson, G. (2001). Electrochemical biosensors: recommended definitions and classification. *Analytical Letters*, 34(5), pp.635-659.

Torre, L. A., Bray, F., Siegel, R. L., Ferlay, J., Lortet-Tieulent, J., & Jemal, A. (2015). *Global cancer statistics, 2012. CA: a cancer journal for clinicians*, 65(2), 87-108.

Tothill, I. E. (2009). Biosensors for cancer markers diagnosis. In Seminars in cell & developmental biology. *Academic Press*, Vol. 20, No. 1, pp. 55-62.

Upadhyay, R. K., & Kumaraswamidhas, L. A. (2018). Bearing failure issues and corrective measures through surface engineering. *In Handbook of Materials Failure Analysis*, pp. 209-233.

Uskoković, V., & Uskoković, D. P. (2011). Nanosized hydroxyapatite and other calcium phosphates: Chemistry of formation and application as drug and gene delivery agents. *Journal of Biomedical Materials Research*, 96(1), 152-191.

Uysal, I., Severcan, F. E., & Evis, Z. A. (2013). Characterization by Fourier transform infrared spectroscopy of hydroxyapatite co-doped with zinc and fluoride. *Ceramics International*, 39(7), 7727-7733.

Vakili, S. N., Rezayi, M., Chahkandi, M., Meshkat, Z., Fani, M., & Moattari, A. (2020). A novel electrochemical DNA biosensor based on hydroxyapatite nanoparticles to detect BK polyomavirus in the urine samples of transplant patients. *IEEE Sensors Journal*.

Walters, M. A., Leung, Y. C., Blumenthal, N. C., Konsker, K. A., & LeGeros, R. Z. (1990). A Raman and infrared spectroscopic investigation of biological hydroxyapatite. *Journal of inorganic biochemistry*, 39(3), 193-200.

Wang, J., & Kawde, A. N. (2001). Pencil-based renewable biosensor for label-free electrochemical detection of DNA hybridization. *Analytica Chimica Acta*, 431(2), 219-224.

Yang, M., & Brackenbury, W. J. (2013). Membrane potential and cancer progression. *Frontiers in physiology*, 4, 185.

Yildiz, U. H., Alagappan, P., & Liedberg, B. (2013). Naked eye detection of lung cancer associated miRNA by paper based biosensing platform. *Analytical chemistry*, 85(2), 820-824.

Yokogawa, Y., Seelan, S., & Zhang, Y. (2006). Hyperstructured hydroxyapatite ceramics as a carrier for cell and protein. *Key Engineering Materials*, 939-942.

Zhang, Q., Chen, C., Xie, Q., & Liu, P. (2009). Electrodeposition of a biocompatible hydroxyapatite matrix to immobilize glucose oxidase for sensitive glucose biosensing. *Microchimica Acta*, 165(1-2), 223-229.

Zhang, X., Guo, Q., & Cui, D. (2009). Recent advances in nanotechnology applied to biosensors. *Sensors*, 9(2), 1033-1053.

Zhao, H. Y., Xu, X. X., Zhang, J. X., Zheng, W., & Zheng, Y. F. (2010). Carbon nanotube–hydroxyapatite–hemoglobin nanocomposites with high bioelectrocatalytic activity. *Bioelectrochemistry*, 78(2), 124-129.

APPPENDIX

APPENDIX A

Operating an Autolab PGSTAT 204

1. The Autolab was turned on with a power switch behind it.
2. Boot computer.
3. Run NOVA 2.0 software on the computer connected to the Autolab.
4. AUT50870 was allowed to upload.
5. Appropriate "actions" were chosen before starting analysis.
6. All data obtained from the various analyses were saved in their appropriate folders before closing the NOVA 2.0 software.
7. Computer was shut down.
8. Autolab was turned off.

Preparation of 5 milimolar Potassium hexacyanoferrate (ferro) in 20mililitre of PBS.

1. 0.033g of $C_6FeK_3N_6$ powder was weighed using a weighing balance and dissolved in 20ml of phosphate buffered saline (PBS) of pH 7.4 and concentration of 0.01M KCl.
2. The solution was shaken to mix completely and placed out of reach from direct sunlight or other light sources to prevent it from reacting with light rays. Fresh preparation of solutions was done daily for every new batch of tests.

Preparation of several concentrations of both commercial and SHAp

1. 20% concentrations of CHAp and SHAp in distilled water were prepared using weight by weight ratios for the concentrations. An empty clean Eppendorf tube was weighed and tarred. 80µl of distilled was weighed and value recorded as Ed. Ed was divided by four to obtain the weight of HAp to be weighed to get 20% HAp. Value of weighed HAp powder was recorded as Ex. Hence 20% concentration of HAp in distilled water solution is obtained by combining Ed to Ex.
2. 10%, 5% and other lower concentrations were prepared from the 20% concentrations of the commercial and in-house prepared HAp's through serial dilutions. 20µl of the 20% HAp solution was pipetted and 20µl of distilled water added to obtain 10% concentration of HAp in distilled water solution. 10µl of the 10% HAp solution was pipetted and 10µl of distilled water was added to obtain 10% concentration of HAp in distilled water solution.
3. Same concentrations of HAp were made replacing distilled water with pedot:pss to obtain a solution of HAp in pedot:pss.
4. All concentrations of HAp prepared were boldly labelled with the right inscriptions for easy identification.

Modification of SPCE surfaces with HAp

1. All solutions of the several HAp concentrations in both distilled water and pedot: pss in their correctly labelled Eppendorf tubes were vortexed to mix properly.
2. SPCEs were labelled accordingly and placed on a horizontal surface.

3. 2µl each of the respective concentrations of HAp were pipetted and coated on the working electrode surface of the spce to form a smooth film. This was carefully performed to avoid contaminating the reference and counter electrode surfaces.
4. The coated spce surfaces were allowed to dry completely for about an hour and half to two hours at room temperature or at least 30 minutes at 70^0C.

Cyclic voltammetry measurement

1. An Autolab potentiostat/galvanostat which is run by NOVA 2.1 software was connected to its power source.
2. A working electrode (red), counter electrode (black), and a reference electrode (blue) connected to the Autolab were properly connected to their terminals and grounded in a faraday cage to prevent external interferences.
3. The 3 electrodes of the composite coated spce surface were properly connected to their respective electrodes of the terminals connected to the Autolab.
4. The coated HAp and Hap/pedot;pss spce surfaces was covered completely with ferro and run on the computer having the NOVA 2.1 software. A bare spce is also covered with ferro and run alongside as the control for the experiment.
5. Working conditions of the NOVA 2.1 software
    I. Applied potential (v) range -0.3v to 0.6v
    II. Step voltage 0.0024v
    III. Start potential 0v
    IV. Scan rate 100mv/s
    V. Working electrode (WE) current 1mA – 100nA
    VI. 2 cycle runs were done for each sample test

APPENDIX B

Table 1 Scan rate analysis data

Scan rate (mV/s)	Voltage range (V)
10	-0.3 to 0.5
20	-0.3 to 0.5
50	-0.3 to 0.5
75	-0.3 to 0.5
100	-0.3 to 0.5
150	-0.5 to 0.7
200	-0.5 to 0.7
250	-0.5 to 0.7
300	-0.5 to 0.7

APPENDIX C

Differential pulse voltammetry (DPV) was performed on the unmodified screen-printed carbon electrode by applying potential within a range of -4 to +0.7 V. DPV is done to determine the potential at which maximum current or electron flow occurs on an electrode surface. A DPV value of 0.098 V is recorded in the voltammogram below, thus the potential at which maximum electron flow occurs on the carbon electrode surface.

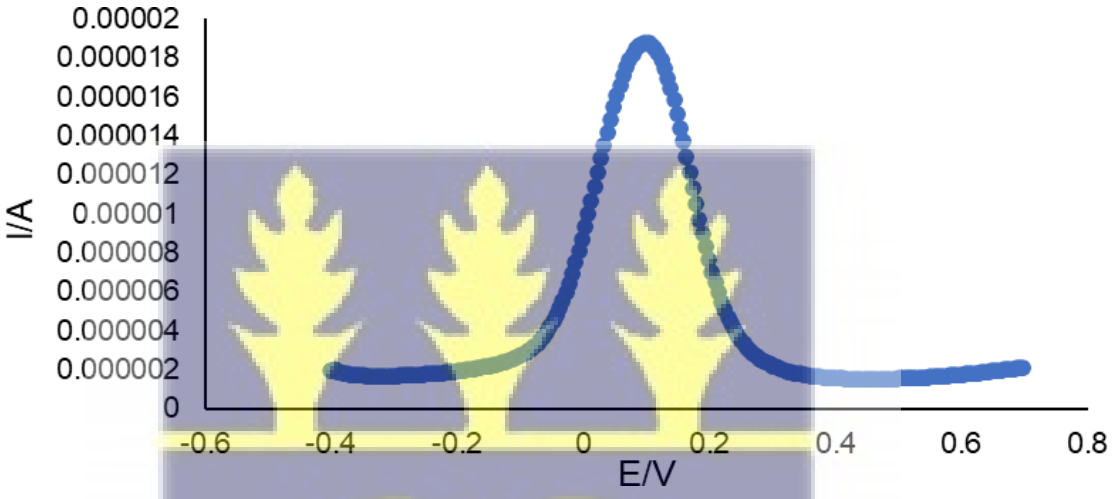

APPENDIX D

Plagiarism Report

Turnitin Originality Report

Processed on: 09-Nov-2020 05:55AM (UTC+0000)

ID: 1440489140

Word count: 16731

Plagiarism check for **"INVESTIGATION OF THE ELECTROCHEMICAL PROPERTIES OF HYDROXYAPATITE IMMOBILIZATION MATERIAL FOR POTENTIAL CYTOSENSOR FABRICATION"** by Adusei Dennis.

Similarity index: 11%

Similarity by source

Internet source: 8%

Publications: 8%

Student Papers: 3%